Available online at www.sciencedirect.com
ScienceDirect
Gondwana Research 12 (2007) 29–46
www.elsevier.com/locate/gr

Nature of mantle source contributions and crystal differentiation in the petrogenesis of the 1.78 Ga mafic dykes in the central North China craton

Peng Peng [a,b,*], Ming-Guo Zhai [a,b], Jing-Hui Guo [a,b], Tim Kusky [c], Tai-Ping Zhao [d]

[a] Institute of Geology and Geophysics, and Key Laboratory of Mineral Resources, Chinese Academy of Sciences, P.O. Box 9825, Beijing 100029, China
[b] Chinese State Key Laboratory of Lithosphere Evolution, P.O. Box 9825, Beijing 100029, China
[c] Department of Earth and Atmospheric Sciences, St. Louis University, St. Louis Missouri 63103, USA
[d] Guangzhou Institute of Geochemistry, Chinese Academy of Sciences, Guangzhou 510640, China

Received 29 March 2006; received in revised form 28 October 2006; accepted 29 October 2006
Available online 20 December 2006

Abstract

Circa 1.78 Ga mafic dyke swarms and some coeval volcanic associations constitute a Large Igneous Province in the central North China craton. The 1st generation of dykes intruded at ca. 1780 Ma and is chemically delineated into 3 groups: the LT Group is gabbroic and has low-Fe–Ti contents, acting as parental magma; the NW Group is high in Fe–Ti-contents and doleritic with an iron-enriched trend; whereas the EW Group is doleritic to andesitic and crystallized from relict siliceous liquids with a silica-enriched trend. They have an EM-I type source and record integral magmatic processes. These include contamination of lithospheric material and assimilation of crustal melts with *in-situ* crystallization in a magma chamber (the LT Group) and fractional crystallization in magma channels (the NW Group) and even with additional alteration (the EW Group). The 2nd generation is slightly younger (ca. 1760 Ma) and scarcely distributed. It has high-Fe–Ti contents, originated from a mixing source of DM and EM-I types. The dykes could be associated with a palaeo-plume: the 1st generation represents lower mantle melts generated from the plume head, whereas the 2nd generation records extra melts from asthenosphere entrained by the plume tail.

Keywords: North China craton; Late Palaeoproterozoic; Mafic dyke swarms; Large Igneous Province; Petrogenesis; Plume

1. Introduction

Mafic dyke swarms are groups of linear mafic intrusions with uniform orientations cutting across various map units and emplaced during a limited time span in certain extension environments, and therefore can act as geological markers. They are abundant in a variety of settings: most large swarms can be related to mantle plumes and are typically associated with divergent plate margins, even contributing to the break-up of supercontinents. Smaller swarms can be associated with volcanic edifices in subduction settings, in back-arc environments, as central complexes related to intrusions, and as an integral component of oceanic crust (Ernst et al., 1995). The ca. 1.78 Ga mafic dyke swarms (Fig. 1), active between 1790 and 1750 Ma and extending for about 1000 km across the central North China craton (NCC), have been suggested to be non-orogenic and related to the continental rifting (Qian and Chen, 1987; Halls et al., 2000; Li et al., 2001; Hou et al., 2001), or post-orogenic activity (Zhao et al., 2001; Wang et al., 2004), or alternatively related to a continental break-up event (Kusky and Li, 2003; Peng et al., 2006). A few geochemical data are reported by Qian and Chen (1987) and Hou et al. (2001) from local areas. Some data from south part of the Taihangshan Mts. are also reported by Wang et al. (2004) with Ar–Ar age constrains. We collected more than 200 dyke samples from north to south of the central NCC (Fig. 1) and carefully selected some of them for chemical analysis. We have reported some major and trace element data in Peng et al. (2004). In a recent paper (Peng et al., 2006), we summarized the age data of the dykes and discussed their tectonic environments. In this paper, we evaluate the roles of crystal differentiation, crustal assimilation and the relative contributions of asthenospheric, lithospheric and lower mantle

* Corresponding author. Institute of Geology and Geophysics, and Key Laboratory of Mineral Resources, Chinese Academy of Sciences, P.O. Box 9825, Beijing 100029, China. Tel.: +86 10 62008082; fax: +86 10 62010846.
E-mail addresses: pengpengwj@mail.iggcas.ac.cn, ppwj@pku.org.cn (P. Peng).

1342-937X/$ - see front matter © 2006 International Association for Gondwana Research. Published by Elsevier B.V. All rights reserved.
doi:10.1016/j.gr.2006.10.022

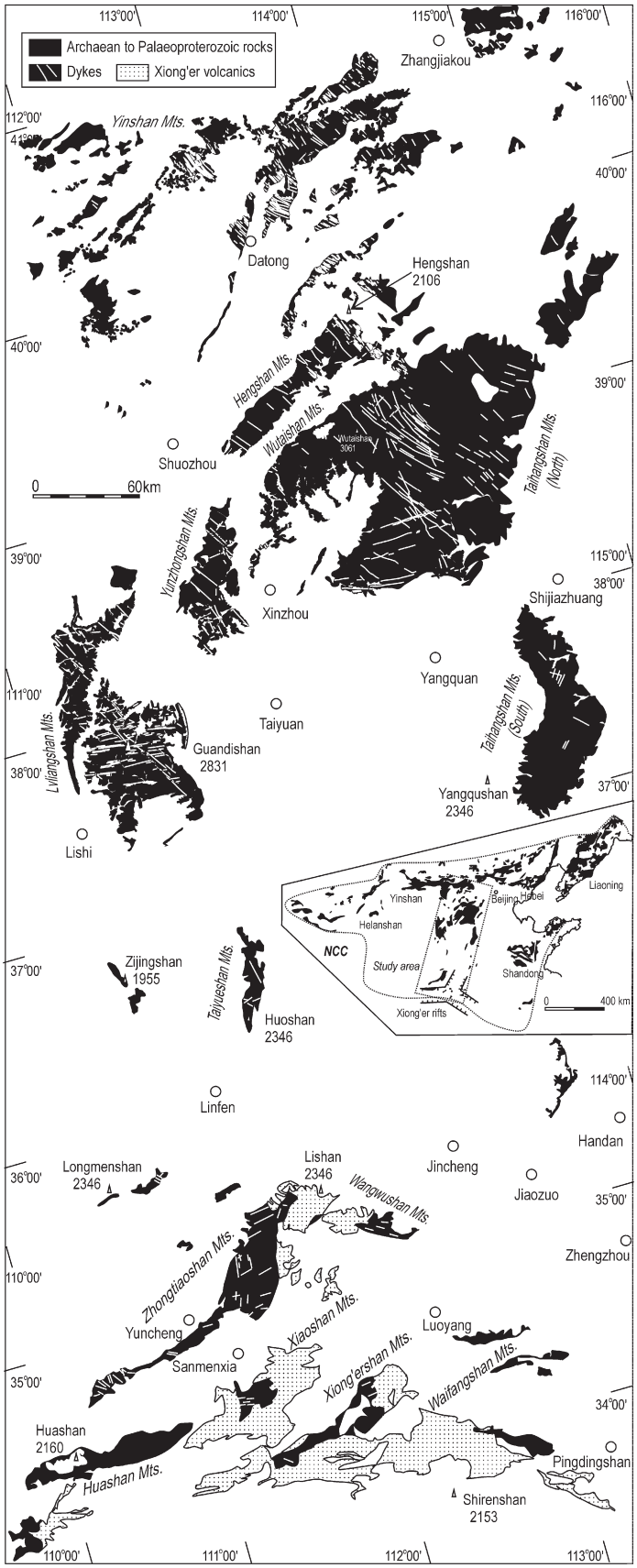

Fig. 1. Simplified geological map of 1.78 Ga mafic dykes in the central NCC.

Table 1
General characteristics and detailed classification of the two dyke generations

Generation	1st generation			2nd generation
Intrusive age	ca. 1780 Ma			ca. 1760 Ma
Groups	LT Gp.	NW Gp.	EW Gp.	HT Gp.
Geochemsitry	Little differentiated Low in Fe–Ti-contents, gabbroic	Highly differentiated High in Fe–Ti-contents, doleritic	Highly differentiated High in Si-content, doleritic to andesitic	Little differentiated High in Fe–Ti-contents, gabbroic
Orientation	N–NW	Mostly N–NW	Mostly E–W	N–NW
Magma source	Similar to enriched MORB; EM I type source			Similar to OIB; Multiple sources: DM+EM I
Samples for major and trace elemental analyses	LT Gp. (4 samples): 01SX025, −36, −37, −40; NW Gp. (32 samples): 01SX009, −10, −11, −12, −15, −16, −18, −20, −26, −27, −32, −39, −41, −46, −47, −54, −65, −67, −73, −79, −82, −85, −86, −87, −90, −92; 02SX028, −29; 03FS01; 03FP04, −05, −07; EW Gp. (7 samples): 02SX001, −04, −07, −08; 03LF01; 03FS07; 03XZ03.			HT Gp. (7 samples): 01SX070; 02SX005, −014, −018, −115; 03HA01; 03WT08.

in the petrogenesis of the dykes with detailed mineralogical and whole-rock major and trace elemental data and isotopic data.

Our results also bear on a current debate on the origin of high-Fe basalts, specifically whether the high Fe is a characteristic of the primary magma or just a result of differentiation. A case study from volcanic rocks at Amisk Lake in Canadian Shield by Leybourne et al. (1999) suggested that the petrogenesis of the high-Fe tholeiitic rocks requires high degrees of partial melting of a dehydrated subducting slab at low pressure. Gibson et al. (2000) suggested that the ferropicrites and high-Fe basalts at the base of the Parana-Etendeka CFB succession in the southern Africa may be derived from Fe-rich streaks in mantle plume starting-heads. However, other researches from the Spiess Ridge segment of the Southwest Indian Ridge and Skaergaard layered complex in the East Greenland support a fractionation origin for ferrobasalts (le Roex and Dick, 1981; le Roex et al., 1982; McBirney, 1989).

There is another old but ongoing controversy whether the tholeiitic liquids evolved to high-SiO_2 and low-FeO^T (total iron, the same as below) liquid (the Bowen trend) or high-FeO^T and low-SiO_2 liquid (the Fenner trend) (Brooks et al., 1991; Wiebe, 1997). Both trends seem to be supported by different study cases (Wiebe, 1997). It is also noted that the magmas on the Fenner trend may still produce extremely small siliceous liquids in the very end stage (McBirney, 1989). Some researches suggested that the

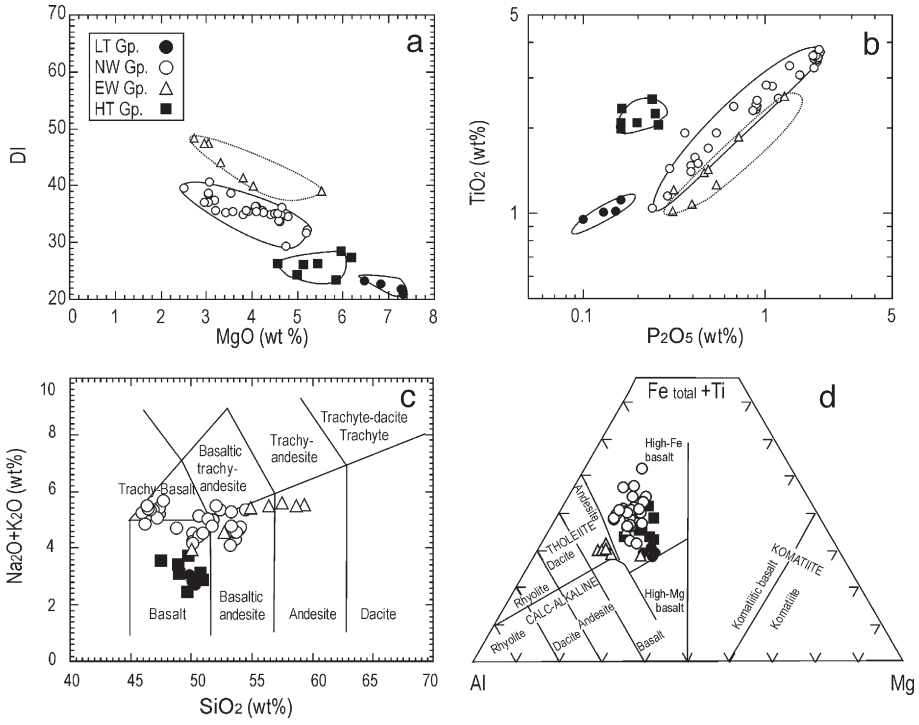

Fig. 2. Classification diagrams for dykes (after Peng et al., 2006, revised): (a) DI (Differentiation Index, DI=Qtz+Or+Ab+Ne+Lc+Kp CIPW norms) vs. MgO, (b) TiO_2 vs. P_2O_5, (c) TAS (SiO_2 vs. (Na_2O+K_2O)), and (d) Fe_{total}+Ti vs. Al vs. Mg (mol) diagrams.

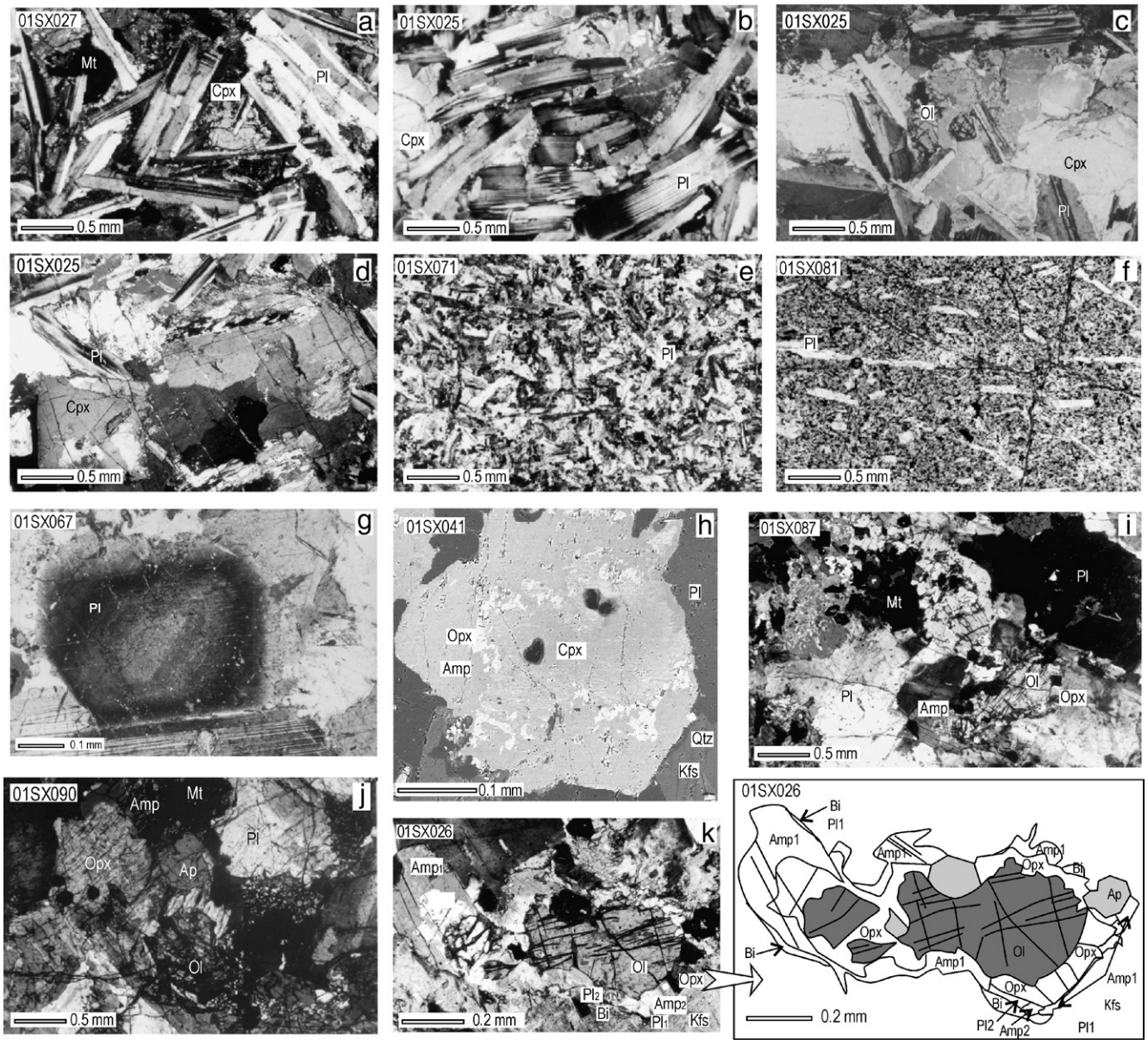

Fig. 3. Typical textures from the thin sections of the dykes showing typical textures of doleritic dykes (a), gabbroic dykes (b, c and d), chilled margins (e and f), plagioclase zoning (g), anetexis of Cpx and Opx (h), and coronas (i, j and k). The abbreviations: Cpx = clinopyroxene; Opx = orthopyroxene; Pl = plagioclase; Mt = magnetite; Ol = olivine; Amp = amphibole; Qtz = quartz; Ap = apatite; Bi = biotite; Kfs = K-feldspar.

tholeiitic magma that differentiates in a closed system at a relatively low oxidation state tends toward the iron enrichment trend, whereas the magma that interacted with the oxidized and hydrated surroundings in the crust tends toward a silica enrichment trend (Brooks et al., 1991). In these processes, the oxygen fugacity controls the fractionation of Fe–Ti oxides (mainly magnetite). Whereas more and more experimental studies (e.g. Juster et al., 1989; Snyder et al., 1993; Toplis and Carroll, 1995, 1996) and case studies (e.g. Hunter and Sparks, 1987; Wiebe, 1997) support that saturation in magnetite will in all cases end Fe-enrichment and cause the fractionating magma to increase in SiO_2. Here the 1.78 Ga mafic dykes provide an example of high-Fe liquids directly produced by differentiation of the normal liquids and crystallized to ferrobasalts and end with siliceous liquids.

2. Geological background

The NCC is composed of two Precambrian blocks, i.e. the Eastern Block and Western Block, separated by the intervening Central Orogenic Belt (COB) (Zhao et al., 1998, 2001; Li et al., 2002; Kusky and Li, 2003; Zhai et al., 2003a). The collision age of the two blocks along the COB is controversial: either at ca. 1.85 Ga (Wu and Zhang, 1998; Zhao et al., 2001; Wilde et al., 2002; Guo et al., 2005; Kröner et al., 2005), or at ca. 2.5 Ga (Kusky et al., 2001; Li et al., 2002; Zhai et al., 2003a; Polat et al., 2005, 2006; Kusky et al., in press-a,b,c). The events during 1.83–1.80 (or 1.79) Ga are extensional (Zhao et al., 2001, 2002a; Li et al., 2002; Zhai et al., 2003a), and the NCC entered into a rift evolution period. There are two main rift systems: the Palaeo- to

Table 2
Selected mineral analyses (wt.%) of dykes

A. Olivine

Sample No.	LT Gp.		NW Gp.				
	01SX025	01SX040	01SX011	01SX020	01SX026	01SX027	01SX087
SiO_2	33.51	32.94	31.94	33.1	30.22	33.27	32.84
TiO_2	0.09	0	0.18	0	0.02	0	0.04
$Al2O_3$	0	0.03	0.03	0.03	0	0.01	0.01
FeO^T	47.82	51.14	53.92	51.51	65.14	50.22	53.03
MnO	0.71	0.72	0.76	0.78	1.27	0.79	0.87
NiO	0.04	0.01	0.05	0	0	0.09	0
MgO	18.23	16.4	14.34	16.5	3.18	17.24	14.50
CaO	0	0	0.02	0	0	0.01	0
Na_2O	0	0.02	0	0.06	0.06	0	0
K_2O	0	0	0.01	0.01	0	0	0
Cr_2O_3	0	0	0	0	0	0	0
Total	100.40	101.30	101.25	101.99	99.89	101.63	101.29
Cation	4 oxygens						
Si	0.993	0.985	0.972	0.983	1	0.986	0.992
Al	0	0.001	0.001	0.001	0	0	0
Ti	0.002	0	0.004	0	0	0	0.001
Fe^{2+}	1.185	1.279	1.373	1.28	1.804	1.244	1.339
Mn	0.018	0.018	0.020	0.02	0.036	0.020	0.022
Mg	0.805	0.731	0.651	0.731	0.157	0.761	0.653
Ca	0	0	0.001	0	0	0	0
Na	0	0.001	0	0.003	0.004	0	0
Ni	0.001	0	0.001	0	0	0.002	0
Total	3.004	3.015	3.023	3.018	3.001	3.013	3.007
Fa	60	64	68	64	92	62	67
Fo	40	36	32	36	8	38	33

B. Plagioclase

Sample No.	LT Gp.			NW Gp.								
	01SX025	01SX036	01SX040	01SX011	01SX020	01SX026	01SX027	01SX065	01SX067	01SX082	01SX085	01SX087
SiO_2	50.96	50.61	52.36	55.09	57.76	60.25	54.3	56.15	57.36	55.37	56.99	56.52
TiO_2	0.03	0	0.10	0.08	0.14	0.05	0.09	0	0.12	0.04	0.13	0.18
Al_2O_3	31.25	31.18	30.69	27.56	26.11	24.62	28.61	27.05	26.65	28.28	27.55	27.17
FeO	0.12	0.01	0.18	0.08	0.21	0.05	0.41	0.08	0.62	0.13	0.47	0.3
MnO	0	0.02	0.05	0	0.04	0	0	0	0	0.05	0	0
NiO	0.03	0.03	0.05	0	0	0.07	0.04	0	0	0	0	0
MgO	0	0.02	0	0.07	0.01	0	0	0	0	0	0.01	0
CaO	13.99	13.61	12.69	10.00	7.62	5.63	10.51	8.90	8.44	9.82	8.78	9.14
Na_2O	3.82	3.78	4.45	6.09	6.98	8.53	5.59	6.69	6.57	6.58	6.48	6.64
K_2O	0	0.03	0.01	0.01	0.08	0	0.05	0	0.39	0	0.10	0
Cr_2O_3	0.13	0.11	0.14	0.15	1.07	0.26	0.54	0.18	0.54	0.17	0.26	0.16
Total	100.33	99.40	100.72	99.13	100.02	99.46	100.14	99.05	100.70	100.40	100.80	100.10
Cation	8 oxygens											
Si	2.315	2.316	2.361	2.506	2.598	2.698	2.457	2.547	2.565	2.489	2.543	2.541
Al	1.672	1.681	1.630	1.476	1.383	1.298	1.525	1.445	1.404	1.497	1.448	1.439
Ti	0.001	0	0.003	0.003	0.005	0.002	0.003	0	0.004	0.001	0.004	0.006
Fe2	0.005	0	0.007	0.003	0.008	0.002	0.016	0.003	0.023	0.005	0.018	0.011
Mn	0	0.001	0	0.003	0	0	0	0	0	0	0	0
Mg	0	0.002	0.001	0.001	0.005	0	0.003	0	0.026	0	0.007	0
Ca	0.681	0.667	0.613	0.487	0.367	0.270	0.510	0.433	0.404	0.473	0.420	0.440
Na	0.336	0.335	0.389	0.537	0.609	0.741	0.490	0.589	0.570	0.573	0.561	0.579
K	0.008	0.006	0.008	0.009	0.061	0.015	0.031	0.010	0.031	0.010	0.015	0.009
Total	5.018	5.008	5.012	5.025	5.036	5.026	5.035	5.027	5.027	5.048	5.016	5.025
Ab	32.8	33.2	38.5	52.0	58.7	72.2	47.5	57.1	56.7	54.3	56.3	56.3
An	66.4	66.2	60.7	47.1	35.4	26.3	49.5	42.0	40.2	44.8	42.2	42.8
Or	0.8	0.6	0.8	0.9	5.9	1.5	3.0	1.0	3.1	0.9	1.5	0.9

C. Clinopyroxene

Sample No.	LT Gp.			NW Gp.								
	01SX025	01SX036	01SX040	01SX011	01SX020	01SX026	01SX027	01SX065	01SX067	01SX082	01SX085	01SX087
SiO_2	51.73	53.15	49.66	51.52	47.68	50.87	49.54	50.61	50.85	49.87	49.66	49.83
TiO_2	0.23	0.13	0.65	0.57	1.82	0.04	1.16	0.54	0.40	0.64	1.05	1.00
Al_2O_3	1.94	1.50	2.97	2.01	4.72	0.37	3.17	2.86	2.68	2.71	2.93	2.77
FeO	8.63	16.43	14.83	11.53	12.98	18.04	12.47	16.71	18.62	15.67	13.00	12.97
MgO	18.27	24.54	13.83	14.45	13.94	8.15	14.46	13.56	12.68	14.22	13.89	14.50

(continued on next page)

Table 2 (*continued*)

C. Clinopyroxene

Sample No.	LT Gp.			NW Gp.								
	01SX025	01SX036	01SX040	01SX011	01SX020	01SX026	01SX027	01SX065	01SX067	01SX082	01SX085	01SX087
MnO	0.25	0.35	0.36	0.36	0.24	0.40	0.26	0.34	0.52	0.37	0.26	0.33
Cr_2O_3	0.27	0.17	0.04	0	0	0.03	0.02	0.05	0.10	0	0.02	0.01
NiO	0	0.02	0.01	0	0	0	0.02	0.02	0	0.03	0.04	0.01
CaO	17.87	4.18	16.13	18.84	17.57	21.16	17.93	16.04	14.68	16.04	18.26	17.25
Na_2O	0.26	0.07	0.24	0.42	0.53	0.32	0.46	0.50	0.40	0.33	0.48	0.38
K_2O	0.01	0	0	0	0	0.01	0.02	0	0.05	0	0.01	0
Total	99.46	100.50	98.72	99.70	99.48	99.39	99.51	101.20	101.00	99.88	99.60	99.05
Cation	6 oxygens											
Si	1.903	1.926	1.896	1.929	1.794	1.990	1.860	1.891	1.921	1.882	1.869	1.884
Al	0.084	0.064	0.134	0.089	0.209	0.017	0.141	0.126	0.119	0.120	0.130	0.123
Ti	0.006	0.004	0.019	0.016	0.052	0.001	0.033	0.015	0.011	0.018	0.030	0.028
Fe^{2+}	0.158	0.421	0.421	0.311	0.271	0.566	0.285	0.425	0.544	0.391	0.303	0.330
Fe^{3+}	0.108	0.077	0.053	0.050	0.138	0.024	0.107	0.097	0.044	0.104	0.107	0.080
Mn	0.008	0.011	0.012	0.011	0.008	0.013	0.008	0.011	0.017	0.012	0.008	0.011
Mg	1.002	1.326	0.787	0.807	0.782	0.475	0.810	0.755	0.714	0.800	0.780	0.817
Cr	0.008	0.005	0.001	0	0	0.001	0.001	0.001	0.003	0	0.001	0
Ni	0	0.001	0	0	0	0	0.001	0.001	0	0.001	0.001	0
Ca	0.704	0.162	0.660	0.756	0.708	0.887	0.721	0.642	0.594	0.648	0.737	0.699
Na	0.019	0.005	0.018	0.030	0.039	0.024	0.033	0.036	0.029	0.024	0.035	0.028
K	0	0	0	0	0	0	0.001	0	0.002	0	0	0
Total	4.000	4.000	4.000	4.000	4.000	4.000	3.999	4.000	3.998	4.000	4.000	4.000
Wo	35.58	8.12	34.15	39.06	37.16	45.12	37.36	33.27	31.06	33.18	38.09	36.08
En	50.61	66.40	40.74	41.69	41.02	24.18	41.93	39.13	37.33	40.92	40.32	42.20
Fs	13.81	25.48	25.11	19.25	21.83	30.70	20.71	27.61	31.62	25.90	21.60	21.72
Jd	0	0	0.67	0.83	0.10	0.57	0.02	0.55	1.46	0.05	0	0.23
Ae	1.94	0.51	1.19	2.31	4.09	1.87	3.52	3.25	1.58	2.49	3.69	2.68

D. Orthopyroxene

Sample No.	LT Gp.		NW Gp.			
	01SX025	01SX040	01sx011	01SX020	01SX027	01SX087
SiO_2	51.75	50.93	51.24	51.14	50.38	51.22
TiO_2	0.03	0.02	0.03	0.01	0.34	0.13
Al_2O_3	0.67	0.58	0.39	0.47	0.69	0.28
FeO	27.87	28.48	29.25	28.49	28.95	29.98
MgO	19.78	19.16	18.32	19.00	15.56	18.12
MnO	0.49	0.59	0.55	0.64	0.72	0.73
Cr_2O_3	0	0.06	0.02	0	0	0
NiO	0.06	0.03	0	0	0.09	0
CaO	0.27	0.41	0.57	0.87	4.63	0.43
Na_2O	0	0.02	0.03	0.01	0.12	0.01
K_2O	0.01	0.02	0.02	0.01	0	0
Total	100.90	100.30	100.42	100.64	101.50	100.90
Cation	6 oxygens					
Si	1.951	1.939	1.958	1.942	1.924	1.954
Al	0.030	0.026	0.018	0.021	0.031	0.013
Ti	0.001	0.001	0.001	0	0.010	0.004
Fe^{2+}	0.811	0.810	0.868	0.808	0.814	0.885
Fe^{3+}	0.068	0.096	0.067	0.096	0.110	0.072
Mn	0.016	0.019	0.018	0.021	0.023	0.024
Mg	1.111	1.087	1.044	1.076	0.886	1.030
Cr	0	0.002	0.001	0	0	0
Ni	0.002	0.001	0	0	0.003	0
Ca	0.011	0.017	0.023	0.035	0.189	0.018
Na	0	0.001	0.002	0.001	0.009	0.001
K	0	0.001	0.001	0	0	0
Total	4.000	3.999	3.999	4.000	4.000	4.000
Wo	0.54	0.82	1.16	1.74	9.36	0.87
En	55.10	53.57	51.68	52.82	43.79	50.81
Fs	44.30	45.61	47.17	45.44	46.85	48.32
Ae	0.06	0.15	0.23	0.08	0.92	0.08

E. Reaction coronas of olivine

Oxide	01SX090								01SX026							
	Ol	Opx	Opx	Opx	Bi	Amp	Pl	Kfs	Ol	Pl_1	Amp_1	Opx	Opx	Bi	Amp_2	Pl_2
SiO_2	29.82	48.11	46.84	50.12	34.65	41.11	64.16	62.39	27.55	60.30	39.69	46.24	45.95	33.59	45.18	63.10
Al_2O_3	0	0.15	0.14	0.79	13.15	9.74	22.76	19.11	0.03	23.60	7.72	0.13	0.06	12.88	6.33	23.29

Table 2 (*continued*)

E. Reaction coronas of olivine

Oxide	01SX090								01SX026							
	Ol	Opx	Opx	Opx	Bi	Amp	Pl	Kfs	Ol	Pl_1	Amp_1	Opx	Opx	Bi	Amp_2	Pl_2
MnO	1.59	1.21	0.91	0.78	0.19	0.23	0	68.00	1.19	0	0.22	1.05	1.04	0.12	0.26	0
FeO	66.12	42.83	43.28	35.71	29.29	27.50	0.31	0	67.19	0.46	27.88	43.94	44.01	30.33	26.72	0.51
MgO	3.01	7.46	7.10	8.17	5.73	5.03	0	0.45	2.82	0.01	4.42	6.65	7.01	5.19	6.55	0.02
CaO	0.02	0.54	1.05	1.40	0	10.52	3.69	0	0.06	5.77	10.19	0.61	0.80	0.01	10.75	3.79
Na_2O	0.02	0	0.03	0.16	0.10	1.75	9.92	0	0	7.78	1.94	0.07	0.04	0.29	1.44	9.18
K_2O	0	0	0.01	0.04	8.82	1.05	0.15	1.56	0.01	0.15	1.19	0	0.01	8.50	0.67	0.33
Cr_2O_3	0	0.09	0	0	0.06	0	0.03	12.77	0.03	0	0.10	0.06		0.09	0.03	0.01
NiO	0.06	0	0.13	0.11	0	0.02	0	0.01	0	0	0	0		0	0	0
TiO_2	0.04	0.03	0.06	0.12	4.68	0.30	0	0.09	0.01	0.03	1.85	0	0.01	4.43	0.78	0.03
Total	100.68	100.42	99.55	97.40	96.66	97.25	101.02	96.38	99.99	99.10	95.10	98.69	98.92	95.35	98.68	100.26
Cation 4 oxygens		6	6	6	11	23	8	8	4	8	23	6	6	11	23	8
Si	0.986	1.986	1.958	2.056	2.750	6.556	2.812	2.959	0.945	2.705	6.540	1.967	1.955	2.724	7.000	2.788
Al	0	0.008	0.007	0.038	1.231	1.830	1.176	1.069	0.001	1.299	1.499	0.006	0.003	1.230	1.156	1.212
Mn	0.045	0.042	0.032	0.027	0.012	0.031	0	0	0.035	0.018	0.031	0.038	0.038	0.008	0.035	0
Fe^{3+}	0	0.016	0.075	0	0	0	0	0	0	0	0.119	0.094	0.134	0	0.140	0
Fe^{2+}	1.829	1.462	1.429	1.225	1.944	3.667	0.011	0	1.926	0.005	3.723	1.468	1.431	2.057	3.322	0.019
Mg	0.149	0.459	0.442	0.497	0.678	1.196	0	0.018	0.144	0.018	1.086	0.422	0.445	0.627	1.513	0.001
Ca	0.001	0.024	0.047	0.062	0	1.798	0.173	0	0.002	0.027	1.798	0.028	0.036	0.001	1.785	0.179
Na	0.001	0	0.002	0.013	0.015	0.542	0.843	0	0	0.676	0.620	0.006	0.003	0.045	0.433	0.787
K	0	0	0	0.002	0.893	0.213	0.009	0.143	0	0.009	0.250	0	0.001	0.879	0.132	0.019
Cr	0	0.003	0	0	0.004	0	0.001	0.772	0.001	0	0.013	0.002	0	0.006	0.004	0
Ni	0.002	0	0.004	0.004	0	0.003	0	0	0	0	0	0	0	0	0	0
Ti	0.001	0.001	0.002	0.004	0.279	0.036	0	0.003	0	0.001	0.230	0	0	0.270	0.091	0.001
Total	3.014	4.001	3.871	3.930	7.807	15.614	5.025	4.964	3.055	4.985	15.909	4.033	4.046	7.841	15.611	5.006

Mesoproterozoic Xiong'er rift system along the southern margin of the craton and elongated into the central NCC was initiated at ca.1.8 Ga (Zhao et al., 2002b, 2004); whereas the Mesoproterozoic intra-continental Yan–Liao rift system along the northern margin and also elongated into the central NCC was initiated at ca. 1.75 Ga (e.g. Wang et al., 1995; Wan et al., 2003). Evidence has also been presented from the NCC to support its involvement in a Palaeoproterozoic supercontinent (Rogers and Santosh, 2002; Zhao et al., 2002a; Wilde et al., 2002; Lu et al., 2002). The break-up time of the NCC from this supercontinent is not well constrained, either 1.6–1.4 (1.2) Ga (Zhao et al., 2002a) or at 1.75 Ga (Peng et al., 2006).

3. Occurrences and generations

Among the Proterozoic dykes of the NCC, the ca.1.78 Ga mafic dyke swarms in the central NCC are the largest, including several hundred N–NW to NW oriented dykes and a few E–W dykes extending across an area of over 100 000 km^2 (Peng, 2005, Fig. 1). The dykes cut no Mesoproterozoic or younger strata, but are contemporaneous with the Xiong'er volcanic rocks in the Xiong'er rift, and could be feeder dykes to these rocks (Peng et al., 2005). Dykes are vertical to subvertical, and in sharp contact with the country rocks with chilled margins. Individual dykes are up to 60 km long and 0.5 to 100 m wide, with mostly around 15 (±5) m wide. The branches of the N–NW-oriented dykes indicate that the magma flow direction is from south to north.

The available zircon and baddeleyite ages cluster around 1780 Ma (1790–1750 Ma) for the dykes (Halls et al., 2000; Peng et al., 2005, 2006). They are classified into two generations according to their ages and occurrences (Table 1). The 1st generation occurred mainly at ca. 1780 Ma, characterized by some reaction coronas in their rocks. They can be further delineated into 3 groups according to their geochemistry (Peng et al., 2006; Fig. 2), i.e. the LT Group (low in Ti–Fe–P-contents, gabbroic, N–NW trending), the NW Group (high in Ti–Fe–P-contents, doleritic, N–NW trending) and the EW Group (high in Si-content, doleritic to andesitic, E–W trending). The 2nd generation could be a little younger, intruding between 1.75–1.78 Ga (at ca. 1760 Ma, Peng et al., 2006) with no reaction coronas in the rocks. They are scarcely distributed in a limited area and simply identified as the HT Group (high in Ti–Fe–P-contents, gabbroic, N–NW trending). The LT and HT Groups were only slightly differentiated and gabbroic in composition, and most are about 20 m in width and more than 10 km in length. They are mainly distributed in a belt of limited area. We

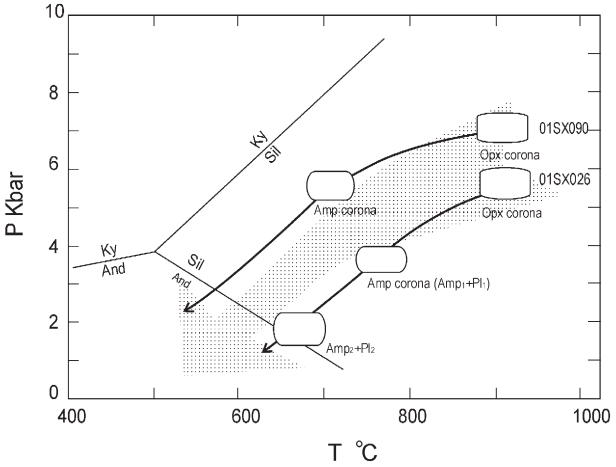

Fig. 4. P–T paths of the 1st dyke generation.

suggest this belt represents the magma chamber orientation, whereas the NW and EW Groups are highly differentiated and doleritic to andesitic in composition, varying in width and length. Among the above 4 groups, the NW Group contains the largest number of dykes and is widespread in the central-western NCC and possibly extends to the eastern NCC. The EW Group is only distributed in the middle part of the central NCC.

4. Petrography and mineral compositions

4.1. Petrography

The primary mineralogy consists of Clinopyroxene (Cpx) and Plagioclase (Pl) and accessory Fe–Ti oxides (Magnetite (Mt) and Ilmenite (Ilm)), Apatite (Ap), Biotite (Bi), K-feldspar (Kfs) and Quartz (Qtz) or Olivine (Ol). The volume of the major minerals is Cpx vs. Pl at about 3:7. Ophitic texture is typical in the NW and EW Groups, whereas equigranular texture is common in the LT and HT Groups. In addition, porphyritic texture is common in the chilled margins and some small dykes (Fig. 3a–f). Pl zoning is generally seen in the NW Group (Fig. 3g). In the 1st generation, a series of reaction textures are observed, including three-stage reactions: Orthopyroxene (Opx, ferrosillite) corona and Amphibole (Amp) corona of Ol and late Amp retrograde assemblage (Fig. 3h–k). There are also Bi coronas of magnetite accompanied with the Ol coronas (Fig. 3i).

4.2. Analytical methods and mineral compositions

Major-element analyses in Table 1A, B, C and D for the minerals were performed on electron microprobe using JXA-8100 at the Key Laboratory of Orogenic Belts and Crustal

Table 3
Selected whole rock Sr–Nd–Pb isotopes of dykes

A. Sr–Nd isotope data

Group	Sample No.	Sr ppm	Rb ppm	$^{87}Rb/^{86}Sr$	$^{87}Sr/^{86}Sr$	2σ	$^{87}Sr/^{86}Sr_t$	Sm ppm	Nd ppm	$^{147}Sm/^{144}Nd$	$^{143}Nd/^{144}Nd$	2σ	εNd_t	T_{DM}
The LT Group	01SX025	318.8	6.42	0.05798	0.706266	12	0.7048	2.27	8.90	0.1545	0.511857	18	−5.62	3.30
	01SX036	339.9	10.08	0.08579	0.707010	13	0.7048	3.01	12.58	0.1450	0.511775	10	−5.05	3.03
	01SX037	341.4	9.35	0.07891	0.706810	14	0.7048	2.91	12.07	0.1457	0.511775	10	−5.21	3.06
The NW Group	01SX011	405.6	40.10	0.28428	0.712487	14	0.7052	11.57	61.38	0.1141	0.511366	13	−5.97	2.71
	01SX020	409.6	43.38	0.30550	0.712974	13	0.7052	11.85	62.40	0.1149	0.511361	14	−6.26	2.74
	01SX047	357.3	28.56	0.23158	0.710824	13	0.7049	4.74	23.40	0.1225	0.511370	10	−7.82	2.96
	01SX082	421.3	49.02	0.33528	0.713638	13	0.7051	9.39	49.10	0.1157	0.511304	10	−7.57	2.85
	01SX086	351.3	45.57	0.37304	0.714691	15	0.7051	12.82	67.82	0.1144	0.511366	9	−6.05	2.72
The EW Group	02SX001	470.4	154.8	0.94409	0.729701	14	0.7055	20.33	113.4	0.1085	0.511287	9	−6.24	2.68
	02SX007	449.8	81.23	0.52048	0.718578	14	0.7053	11.32	62.60	0.1094	0.511285	10	−6.49	2.71
	03LF01	448.9	74.42	0.48172	0.716187	13	0.7039	8.36	45.14	0.1121	0.511358	17	−5.68	2.67
	03FS04	228.5	131.8	1.65706	0.743990	12	0.7016	17.52	101.9	0.1041	0.511270	10	−5.55	2.60
	03FS07	538.7	106.0	0.56924	0.718516	13	0.7039	11.08	62.74	0.1069	0.511297	13	−5.68	2.63
The HT Group	02SX018	223.1	46.82	0.60524	0.718630	13	0.7033	4.52	18.13	0.1511	0.512165	12	1.60	2.39
	02SX115	257.2	40.39	0.45110	0.713806	15	0.7024	4.96	19.72	0.1523	0.512204	10	2.07	2.34
	03WT08	338.6	46.09	0.39124	0.712408	11	0.7025	4.65	18.32	0.1535	0.512236	9	2.44	2.30
	02SX005	309.4	39.69	0.36820	0.715712	9	0.7064	6.08	28.28	0.1300	0.512174	10	6.54	1.77
	02SX014	291.1	66.44	0.65577	0.718683	10	0.7021	6.01	27.92	0.1302	0.512161	10	5.25	1.80

B. Pb isotope data

Group	Sample No.	Th ppm	U ppm	Pb ppm	$^{208}Pb/^{204}Pb$	$^{208}Pb/^{204}Pb_t$	2σ	$^{207}Pb/^{204}Pb$	$^{207}Pb/^{204}Pb_t$	2σ	$^{206}Pb/^{204}Pb$	$^{206}Pb/^{204}Pb_t$	2σ	μ	κ
The LT Group	01SX025	0.43	0.11	1.74	36.7300	35.12	16	15.3832	15.23	14	16.6364	15.21	12	4.5	3.9
	01SX036	0.82	0.63	6.14	37.3088	36.44	15	15.4574	15.37	15	16.7282	15.96	13	2.4	1.3
	01SX037	0.81	0.20	3.03	37.1193	35.37	30	15.4177	15.26	29	16.8539	15.37	27	4.7	4.1
The NW Group	01SX011	2.65	0.65	8.97	36.6866	34.76	7	15.3651	15.19	8	16.6024	14.97	7	5.1	4.1
	01SX020	2.61	0.70	10.10	36.8212	35.13	16	15.3965	15.23	15	16.6155	15.05	14	4.9	3.7
	01SX047	2.79	0.58	7.06	38.2464	35.67	11	15.5323	15.33	11	17.2360	15.38	11	5.8	4.8
	01SX082	3.66	0.59	11.5	37.2973	35.22	18	15.4158	15.29	17	16.4990	15.34	17	3.6	6.2
	01SX086	2.67	0.59	11.0	36.5267	34.94	14	15.3474	15.22	14	16.3680	15.16	13	3.8	4.5
The EW Group	02SX001	4.23	0.91	23.0	36.1347	34.93	13	15.2392	15.14	13	16.9993	16.11	13	2.8	4.6
	02SX007	5.15	0.89	19.9	36.5530	34.86	12	15.2033	15.09	11	16.0439	15.04	11	3.2	5.8
	03LF01	1.40	0.60	12.3	36.6947	35.95	11	15.2394	15.12	9	16.1230	15.02	8	3.5	2.3
	03FS04	6.09	1.21	24.9	35.9304	34.33	8	15.1283	15.01	7	15.5632	14.47	8	3.4	5.0
	03FS07	4.89	0.87	14.0	35.9395	33.66	12	15.1872	15.03	12	15.7570	14.36	12	4.4	5.6
The HT Group	02SX018	2.51	0.48	8.06	37.8974	35.89	17	15.5288	15.39	14	17.5682	16.24	13	4.2	5.2
	02SX115	2.71	0.55	5.39	39.1483	35.90	11	15.6198	15.38	10	18.5257	16.25	10	7.2	4.9

Note: Initial data calculated assuming a forming age of 1780 Ma for the 1st generation (the LT, NW & EW Groups) and 1760 Ma for the 2nd generation (the HT Group).

Evolution, Peking University. The accelerating voltage was 15 kV, and the analyzing current was 10 nA. The standard samples were from SPI Company in America. Whereas the data in Table 1E are obtained using CAMECA SX51 at Institute of Geology and Geophysics, Chinese Academy of Sciences (CAS). The accelerating voltage was 15 kV, and the analyzing current was 12 nA. The standard samples were from P and H Development Company in British. In both laboratories, the precise was about ±1.5% for a concentration of 1 wt.% relatively. See data in Table 2.

4.2.1. Olivine (Ol)

Ol generally has reaction coronas companying the accessory minerals in the NW Group dykes (Fig. 3i–k). It rarely happens in the LT Group, only appearing as tiny inclusions in the Pl or Cpx minerals. No Ol is found in the HT and EW Groups. The Ol is greenish in color and small in size (about or less than 1 mm). The composition of the Ol ranges from Fo_8 to Fo_{40}, mostly between Fo_{32} and Fo_{40}, showing characteristics crystallized from highly differentiated liquids.

4.2.2. Plagioclase (Pl)

Pl is the major mineral phase, always composing more than 60 volume % of the mineralogy of the dykes. Its composition varies from An_{26} to An_{66}: An_{26} to An_{50} for the doleritic dykes (the NW and EW Groups) and over An_{50} for the gabbroic dykes (the LT and HT Groups). Zoning of Pl in the NW Group shows a steady differential crystallization process (Fig. 3g).

4.2.3. Clinopyroxene (Cpx)

The composition of Cpx ranges between $Wo_{31(8)–45}$, $En_{37(24)–51(66)}$ and $Fs_{14–27}$, mostly belonging to augite. The TiO_2 (0.1–1.8 wt.%) and Al_2O_3 (1.5–4.7 wt.%) contents are varied. Cpx sometimes appears as sub-grains (Fig. 3d), being possibly related to the recrystallization during uplifting.

4.2.4. Auxiliary minerals (Fe (–Ti) oxides, Ap, Qtz and Kfs)

Fe (–Ti) oxides are mostly Mt with some Ilm. The portion of Fe (–Ti) oxides is around 5 volume % for doleritic dykes (the NW and EW Groups). Kfs is rarely seen only in some dykes of the NW and EW Groups, whereas Ap is common as inclusions in the minerals and intergrowth with Ol coronas. Qtz is generally seen in doleritic dykes, with a volume portion of less than 5% in general, and over 5% in a few andesitic dykes.

4.2.5. Reaction coronas

Opx and Amp reaction coronas of Ol, Opx coronas of Cpx and Bi coronas of Mt are observed in the 1st generation dykes (Fig. 3h–k). The compositions of related minerals are listed in Table 1D and E. These minerals are obviously high in FeO^T-content but low in MgO-content, showing characteristics inherited from Ol. In some coronas, there are late-stage Amp_2 and Pl_2, with different compositions from the coronas (Amp_1 and Pl_1) (Fig. 3k). There are also some Opx solid solution bands and pieces in and around Cpx, representing anatectic processes (Fig. 3h). Similar Ol, Cpx and Mt corona textures are discussed by Markl et al. (1998) in detail and suggested to be reactions under granulite-facies during the last stages of magmatism. We can identify three-stages of metamorphism: the first stage Opx corona presents products of reaction between Ol and Pl; the second stage Amp_1 is retrograde metamorphosed products of Opx; whereas the last stage Amp_2+Pl_2 represented another retrograde metamorphism event. Thermo-barometer calculations using Opx thermometer of Brey and Kohler (1990) and barometer of Bohlen and Batcher (1981) for the first stage, and

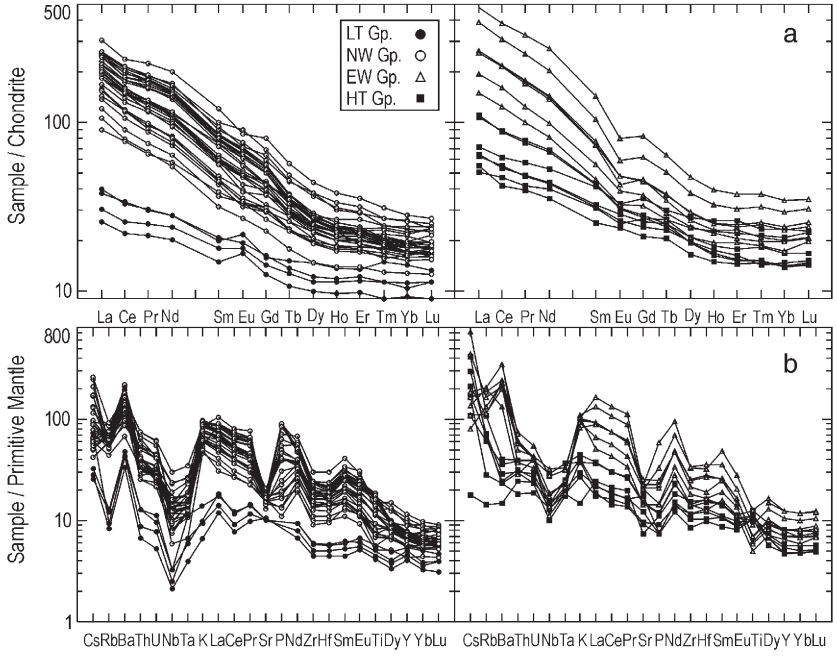

Fig. 5. (a) Chondrite-normalized REE patterns, and (b) Primitive mantle-normalized multi-element spidergrams of dykes (Chondrite and primitive mantle-normalized values of Sun and McDonough, 1989).

Amp-Pl thermometer of Blundy and Holland (1990) and Amp barometer of Hollister et al. (1987) for the second and third stages reveal an uplifting process for the dykes from an emplacement depth of up to 20 km to several kilometers with the wall-rocks (Fig. 4).

5. Bulk rock compositions

5.1. Analytical methods and selected samples

All the bulk compositions were analyzed in the laboratory at Institute of Geology and Geophysics, CAS. Major element determinations were performed by X-ray fluorescenece after fusion with lithium tetraborate using Chinese national standard sample: GBW07101-07114. The precision was better than 0.2 wt.% in the analysis range. The Loss On Ignition (LOI) contents of the samples were measured as the weight loss after one hour's baking under a constant temperature at 1000 °C. Trace element analyses were finished by Inductively Coupled Plasma Mass Spectrometer (ICP-MS) after HNO_3+HF digestion of about 40 mg sample powder in a Teflon vessel. This analysis was performed on an ELEMENT spectrometer using Chinese national standard samples GSR1 (granite), GSR2 (rhyolite) and GSR3 (basalt). The Relative Standard Deviation (RSD) was better than 5% above the detection limits. The data were published in Peng et al. (2004) (the samples were re-sorted by generations and groups in Table 1).

Sr–Nd–Pb isotope determinations were performed on a Finnigan MAT 262 spectrometer after elements were separated by ion-exchange resins using reference standards NBS987 (Sr standard), Ames (Nd standard) and NBS981 (Pb standard). Standard material BCR-1 (basalt powder) was processed and analyzed with the selected samples to check the procedure. The whole procedure backgrounds for Rb–Sr, Sm–Nd and Pb isotope analyses were better than 100 pg, 50 pg and 50 pg, respectively. The external precision (2σ) of $^{87}Rb/^{86}Sr$ and $^{147}Sm/^{144}Nd$ proportion was better than 0.5%. The chemical procedure and detailed analysis conditions were the same as in Chen et al. (2000). See data in Table 3.

5.2. Major and trace element geochemistry

In the classification diagrams, the LT and HT samples plot in the field of tholeiitic basalts (Fig. 2c, d). The NW Group exhibits a negative correlation between total alkaline and SiO_2 (Fig. 2 c). The correlation of K_2O with SiO_2 is considerably better than with Na_2O. The EW Group shows a positive correlation in this same diagram. The high K_2O content even into the alkaline field is due to highly differentiated nature of the liquid under an iron-enriched and silica-poor trend. This strong differentiation trend is obviously shown in Fig. 2ab. The Mg-numbers (simplified as Mg#, calculated assuming Fe^{2+}=0.85 * total Fe) of the rocks range from 0.54–0.57 for the gabbroic dykes (the LT and HT Groups) and 0.26–0.49 for the doleritic dykes.

The rocks show variable REE patterns, i.e. the LT Group shows light enriched patterns while the other 3 Groups have medium to high LREE enriched patterns with higher REE-contents (Fig. 5). The $(La/Yb)_N$ values are 2.5–3.4, 2.3–7.5, 4.6–12.8 and 8.1–13.1 for the LT, HT, NW and EW Groups, respectively. The LT Group shows positive Eu anomalies; the NW Group shows small anomalies; whereas the EW Group shows negative Eu anomalies. The HT Group has both light positive and negative anomalies.

The NW and EW Groups have higher trace element contents than the LT Group. They are all enriched in Ba and K, but depleted in Rb and most HFSEs (high field strength elements, e.g. Th, U, Nb, Ta, Zr, Hf) compared to the neighbouring elements in the multi-element spidergram (Fig. 5). The NW and EW Groups also show LREE enrichment and variable P-content. The HT Group shows weaker depletion and enrichment. They are enriched in Cs, Rb, K and Ti, but slightly depleted in Nb. The variation of the Sr- and P-contents could be caused by differentiation. The Zr/Sm and Nb/La values for the HT Group are 23.5–27.8 and 0.56–0.81, respectively, similar to

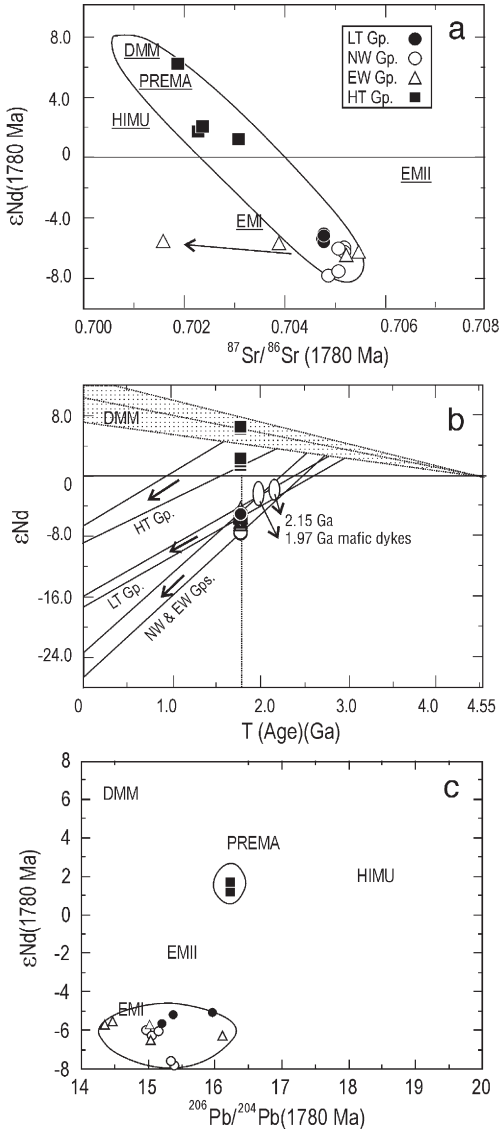

Fig. 6. (a) $^{87}Sr/^{86}Sr_t$ vs. εNd_t, (b) Nd isotopic evolution, and (c) εNd_t vs. $^{206}Pb/^{204}Pb_t$ diagrams of dykes. Data of 1.97 Ga and 2.15 Ga dykes are of our unpublished results.

the OIB (28, 1.297) or PM (25.5, 1.08). These values are lower for the LT Group, i.e. 15.2–16.1 and ~0.2. The Nb/U, La/Nb and Zr/Ba ratios are 2.9–10.7, 4.95–5.24 and 0.18–0.20 for the LT Group and 15.0–24.7, 1.23–1.79 and 0.57–0.81 for the HT Group, suggesting strong crustal influence for the LT Group and also some influence for the HT Group.

5.2.1. Sr–Nd–Pb isotope geochemistry

The analytical results of the whole rock Sr–Nd–Pb isotopes for selected samples are shown in Table 3A, B. The $^{87}Sr/^{86}Sr_t$ values of the LT Group dykes are restricted around 0.7048. The εNd_t values ranges from −5.05 to −5.62. Their $^{206}Pb/^{204}Pb_t$ values are 15.2–16.0. While the $^{87}Sr/^{86}Sr_t$, εNd_t and $^{206}Pb/^{204}Pb_t$ values of the NW Group samples are 0.7049–0.7052, −5.97–−7.82 and 15.0–15.4, respectively. The εNd_t of the EW Group dykes are similar to the NW Group, but the $^{87}Sr/^{86}Sr_t$ values are variable from 0.7016 to 0.7055. This could be due to late stage erosion which caused radiogenic Sr loss and decreased the $^{87}Sr/^{86}Sr$ ratios, or contamination of Rb-bearing melts which heightened the Rb contents and the $^{87}Rb/^{86}Sr$ values. The HT Group shows two subgroups: one has εNd_t of about 6.20 and $^{87}Sr/^{86}Sr_t$ at about 0.7021, while the other one at 1.60–2.40 and 0.7024–0.7033. Their $^{206}Pb/^{204}Pb_t$ values are both at about 16.2. The magma source of the 1st generation (the LT, NW and EW Groups) is affinitive to an EM-I type, i.e., a very uniform enriched mantle source, whereas the 2nd generation (the HT Group) is similar to a PREMA-DM type (Fig. 6).

6. Discussion and conclusions

6.1. Differentiation processes

For the 1st generation, the NW and EW dykes experienced significant removal and crystallization of Ol, Pl and Cpx. This is shown in the trace element correlation diagrams (Fig. 7) and the Pearce ratio diagrams (Fig. 8). Pearce's element ratios, named after T.H. Pearce, can test whether the members of a rock suite are comagmatic or not, and can illustrate the causes of chemical diversity in a comagmatic suite (Pearce et al., 1975; Russell and Nicholls, 1988). These diagrams reveal that Pl is the main fractionated phase. We processed a synthesis crystallization model for the 1st generation with various differentiation processes (Figs. 9–11). From these models, an equilibrium crystallization or *in-situ* crystallization process cannot alone explain the diversities in each group or the differences among the 3 groups. It is also shown that the fractional crystallization process could be the most important process. But a fractional crystallization process can not explain the different REE-patterns between the LT Group and the NW and EW Groups (Fig. 5). The possible interpretation for the differences is that the rocks do not belong to a same comagmatic suite but were originated from different sources, or the differences are caused by different degrees of crustal assimilation/magma mixing, or result from certain source with different degrees of partial melting of some HREE-bearing accessory minerals. Alternatively, we suggest that they belong to a comagmatic suite as they show similar isotope values and trace element patterns and continuous changing elemental contents. The diversity in REE patterns could be initiated by certain equilibrium or *in-situ* crystallization processes in the upper magma chamber (Fig. 10).

We present here a possible model of crystallization processes for the 1st generation dykes, including *in-situ* crystallization and fractional crystallization of Ol+Cpx+Pl (Fig. 11a, b). This model fits well with most trace element patterns of the samples except the Ti-content, which is possibly controlled by the crystallization of Ilm and Mt. The variation of some trace elements in the EW Group could be controlled by late stage contamination or erosion, a contention supported by the Sr–Nd isotopes. The LT Group is the parental magma of the NW and

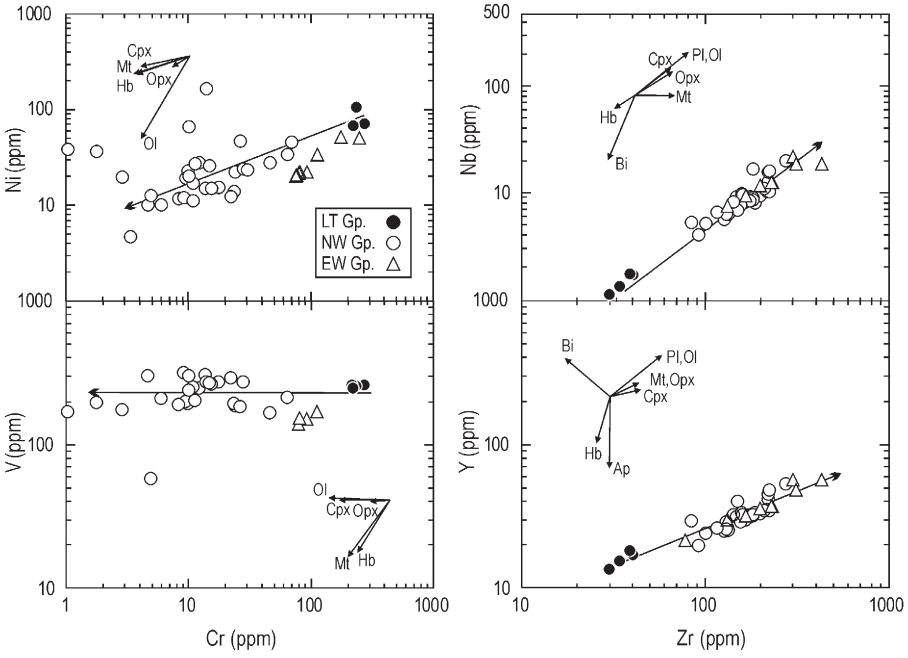

Fig. 7. Bivariant plots showing fractionation trends of the 1st dyke generation.

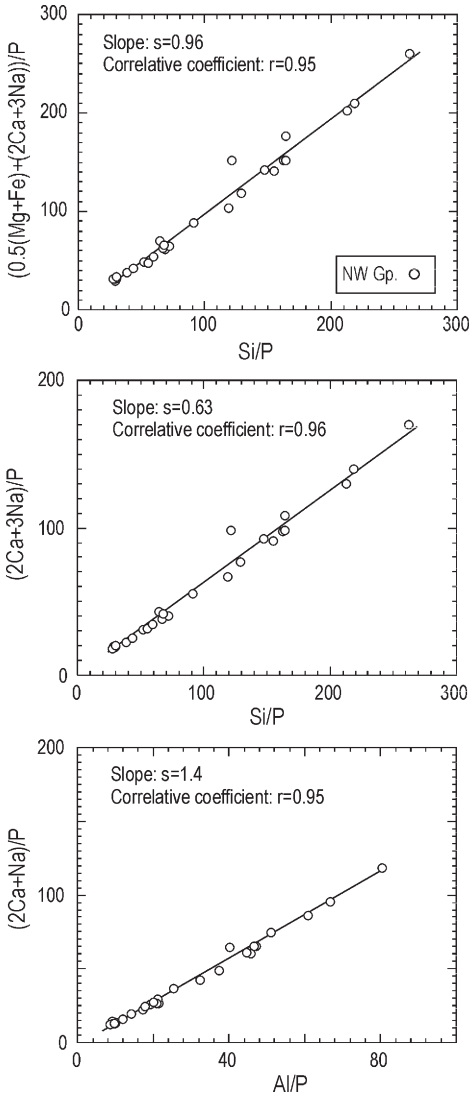

Fig. 8. Diagrams showing the Pearce's element ratios of the NW Group dykes. Phosphorus is selected as incompatible element here. The ratios are calculated in molecular using the whole rock composition. The slopes in the (2Ca+3Na)/P vs. Si/P and (2Ca+Na)/P vs. Al/P diagrams will tend to 1 if Pl is the sole crystallizing and segregating phase. The slope in the 0.5(Mg+Fe)/P vs. Si/P diagram tend to 1 when the Ol is the corresponding sole fractionated phase. And if the Cpx is the right phase, the slope in the (2Ca+Na)/P vs. Al/P will approach to ∞.

EW Groups, but it is not qualified as primitive magma. It could be a composition produced through mixing of a periodically refilling primary magma with the differentiated magma in the chamber. The enriched characteristics of the Ba in Fig. 5 could be the result of contamination or mixing of melts from phlogopite-rich veins in the lithosphere (Peng, 2005). For the 2nd generation (the HT Group), only a few samples are available. These samples show correlative Eu and Sr anomalies (Fig. 3), showing possible Pl-fractional crystallization.

There are only small variations in composition along the orientation of dykes. But the compositions are quite varied from the margin to the interior of an individual dyke, i.e., it is higher in REE- and incomparable element-contents and lower in MgO-content and more depleted in Sr-content in the margin than the interior. This may be caused by quick solidification of the melts in the margin without early Pl-accumulation. They have similar patterns in chondrite-normalized REE patterns and the primitive mantle-normalized multi-element spidergram, suggesting little contamination in the magma channels during crystallization. The possible assimilation could have happened before the magma reached the channels.

6.2. Genesis of high-Fe–Ti basalts (the NW Group)

The NW Group dykes are ferrobasalts in composition; they have high Fe- and Ti-contents, with up to 19.06 wt.% of FeO^T and 3.78 wt.% of TiO_2. Among the main Fe- and Ti-bearing minerals, i.e. Cpx, Ilm and Mt, Cpx is the major silicate component. But the Fe- and Ti-contents in the Cpx are nearly oppositely related to the counterpart compositions of the whole rock (Fig. 12). So the variations of the Fe- and Ti-contents are not controlled by silicates and could be essentially controlled by oxides (Ilm and Mt). The NW Group samples present a Fenner differentiation trend, i.e. the iron-rich and silica-poor fractional crystallization trend; whereas the EW Group appears as a Bowen trend, i.e. the iron-poor and silica-rich process. The former trend is thought to be formed by differentiation of magma in a closed system at a relatively low oxidation state (Brooks et al., 1991). In such magmas, iron concentrates in late crystals. Ol is high in Fe-content and its composition cannot be in equilibrium with the whole rock. We think Ol crystallized from the trapped high-Fe relic liquids in-between the framework of Pl in the very late stages, accompanying with Mt and Ilm. Compositionally, the NW Group dykes are descendents of the LT Group. The high-Fe characteristic could also be generated through Fenner trend differentiation of the LT Group dykes. The N–NW and E–W Groups are generated from the same magma source according to our chemical and isotopic data. Two kinds of differentiation trends are also reported to appear together in the Emeishan flood basalts and thought to be controlled by crustal assimilation, which could possibly cause differences in oxygen fugacity (Xu et al., 2003). Both the NW and EW Groups show assimilation characteristics. The continuously changing trace element patterns for the dykes except for some alteration-related variation indicate possibly no large differences in degrees of assimilation. Therefore we think it is hard to explain the changing of the differentiation trend by oxygen fugacity variation by assimilation. As the Fenner trend may still produce siliceous liquid when Mt is saturated (e.g. Hunter and Sparks, 1987; Juster et al., 1989; McBirney, 1989; Snyder et al., 1993; Toplis and Carroll, 1995, 1996; Wiebe, 1997), the EW Group might crystallize from a siliceous liquid produced after separation of the NW Group from the parental magma.

6.3. From the 1st generation to the 2nd generation: changing of the mantle sources

In the 1st generation, the NW and EW Groups are the descendents of the LT Group. The different chemical characteristics of the EW and NW Groups are due to different differentiation degrees and trends, together with possible assimilation

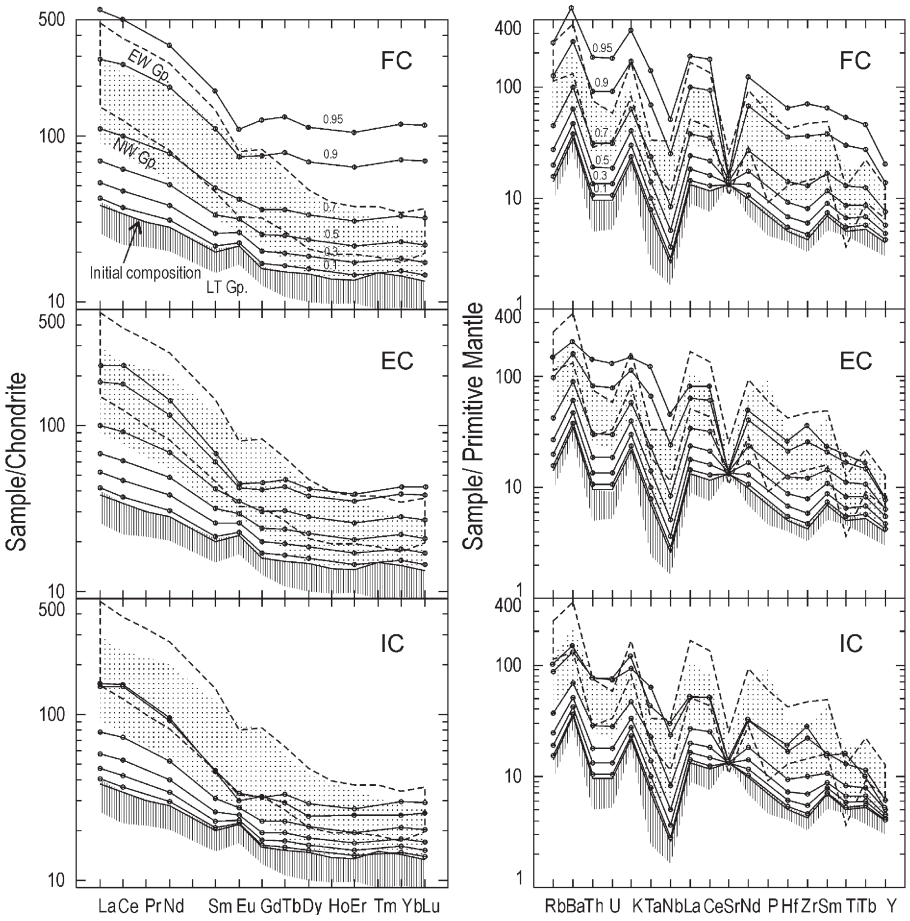

Fig. 9. Crystallization modelling calculation of varies processes at a fixed fractional mineral combination for the 1st generation dykes, i.e. 1:1 Pl and Cpx, assuming fraction ratio at 95%, 90%, 70%, 50%, 30% and 10%. The curves with black circles show simulated compositions after crystallization from sample 01SX040. FC: Fractionated Crystallization; EC: Equilibrium Crystallization; IC: *in-situ* Crystallization. The area filled with vertical lines represents the LT Group, the area with dots refers to the NW Group, and the dotted line circled area refers to the EW Group. The partition coefficients are cited from Rollinson (1995) (for basaltic and basaltic andesite liquids). Chondrite and primitive mantle normalized values of Sun and McDonough (1989).

and alteration. So the LT Group can represent the characteristics of the magma source of the 1st generation. The two generations (the LT and HT Groups) show two distinctive kinds of basalts: low-Fe–Ti and high-Fe–Ti basalts, respectively. Two kinds of basalts are also reported together in other Large Igneous Province (LIP) such as the Deccan, Karoo, Parana and Indo-China LIPs, suggested to be from different sources (Mahoney, 1988; Gallagher and Hawkesworth, 1992; Hoang et al., 1996). Elementary and isotopic geochemistry characteristics indicate that the LT and HT Groups could not be generated through differentiation or assimilation of crustal materials from one source. They are inherited from different mantle sources. The LT Group shows EM-I mantle source isotopic characteristics (Fig. 6). EM-I type source is thought to be a slightly modified bulk earth component; it could reside in the subcontinental lithosphere, in the lower mantle, or in a core/mantle boundary layer (e.g. Hart, 1988). Former studies reveal that the lithospheric mantle could not be the source of continental basalts, especially for those that have depleted Nb and Ta contents and high Sr and low Nd isotope ratios (Arndt and Christensen, 1992; Menzies, 1992). In addition, melting of lithospheric mantle might not produce such large volume basalts with uniform geochemistry over such a broad area. We suggest that the EM-I source component of the LT Group could be from the lower mantle (including the core/mantle boundary) rather than lithospheric mantle. The HFSE depletion characteristics could be produced by assimilation and contamination of crustal and lithospheric melts. The crustal rocks in the study area have close εNd_t values with the dykes (Fig. 13, database of Wu et al., 2005), and assimilation of the crustal melts can not significantly change this value. It possibly represents their original values even with crustal assimilation. The HT Group shows a pattern close to OIB in the trace element spidergram (Peng et al., 2006). The OIB-like end member, showing DM mantle characteristics, may have come from asthenospheric mantle, mixed with a lower mantle source and become contaminated by lithospheric melts. So the predominant mantle source could have changed from lower mantle to asthenospheric mantle from the LT Group (the 1st generation) to the HT Group (the 2nd generation).

6.4. A palaeo-plume associated genesis and geological implications

The 1.78 Ga dyke swarms are widespread in the central NCC and possibly also in the eastern and western parts of the craton. They can be called as the North China giant mafic dyke swarms

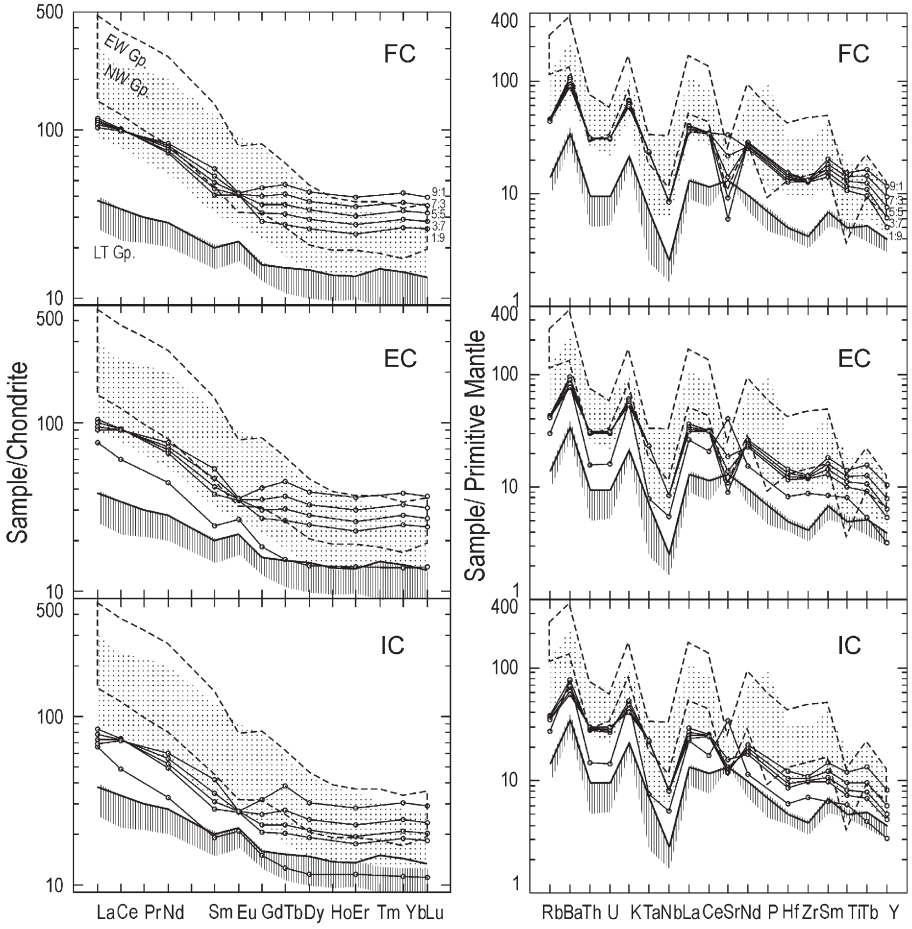

Fig. 10. Crystallization modelling calculation with assumed differentiation trends at fixed magma fraction. The curves with black circles show simulated compositions after 50% crystallization from sample 01SX040 in fixed ratios of Pl and Cpx at 9:1, 7:3, 5:5, 3:7 and 1:9. Other information is the same as in Fig. 9.

rather than as Taihangshan–Hengshan dykes by Halls et al. (2000). Peng et al. (2006) have reconstructed the dykes and concluded that the N–NW dykes in the central and western NCC (the LT, NW and HT Groups) constitute a fanning geometry with their apex pointing to the Xiong'er rift centre (Fig. 14a), feeding the Xiong'er volcanic association. In the central NCC, the dyke swarms have an extent scale of nearly 1000 km and over an area of more than 100 000 km^2, whereas the volcanic association with some related ultramafic rocks are distributed in an area of over 60 000 km^2. Together they constitute a LIP. We are not sure whether the Xiong'er volcanic association is a silicic LIP, or a mafic LIP with some mafic parts lost to erosion as it appears to be silicic dominated with a few mafic rocks. Giant fanning geometry is always found in plume-related dyke warms (e.g. Mackenzie, Matachewan and Yakutsk dyke swarms, and the Central Atlantic reconstructed dyke swarms, see Ernst et al. (1995) and references therein). According to Ernst et al. (1995), those dykes that are associated

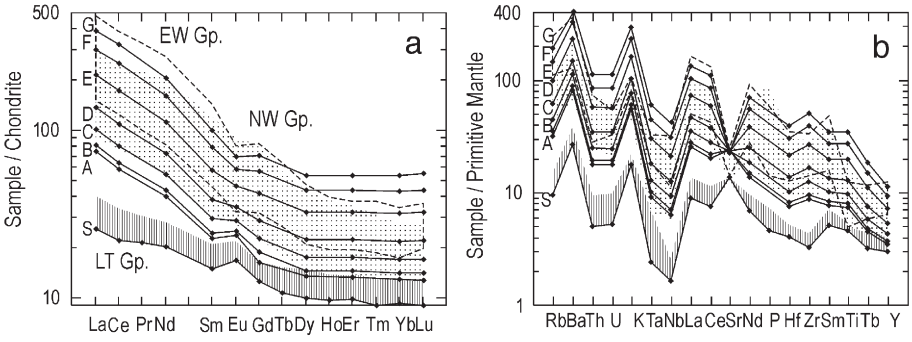

Fig. 11. Crystallization modelling calculation for the dykes of the 1st generation. (a) REE patterns, and (b) trace element spidergram. Curves A, B, C, D, E, F and G refer to simulated compositions after 75% *in-situ* crystallization of Cpx+Pl+Ol at 70:20:10, 10%, 30%, 50%, 70%, 80% and 85% fractional crystallization of Pl+Cpx +Ol at 55:35:10, respectively. S represents the start composition for calculation. Other information is the same as in Fig. 9.

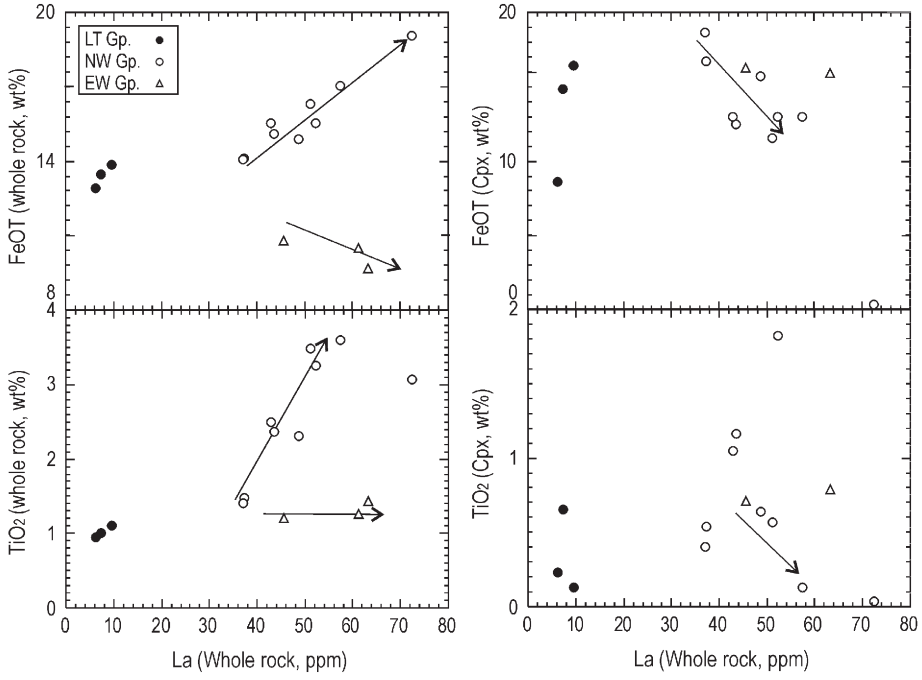

Fig. 12. FeO^T and TiO_2 abundances in Cpx and whole rock compare to the corresponding La-content.

with plumes have an averaging thickness of 20 to 40 m, in contrast to values of 0.5 to 2 m for those from volcanic edifices, intrusive centers and ophiolites. Abbott and Isley (2002) further suggested that the widest feeder dykes from a superplume is typically >70 m. The dykes here have widths of up to 100 m, averaging 15 m, and they are more likely to be associated with a plume.

Moreover, the mantle plume-related volcanic associations and dykes have a number of characteristics that are distinguished from others, including uplift prior to volcanism, dyke orientation, physical volcanism, age progression along hotspot tracks and the chemical characteristics of the magma (Compbell, 2001). Firstly, in the central NCC, uplift occurred at ca. 1.80 Ga, and is represented by the granitic intrusions, the extension structures and retrograde metamorphism. Uplift happened before and was coeval with the volcanism. Secondly, the dyke orientation agrees with a plume genesis (Peng et al., 2006). Thirdly, for the physical aspects of the volcanic rocks, the stratigraphy of the volcanics is not pyroclastic deposit dominated, and the composition is correlated in large area (Zhao et al., 2002b). The dykes even track for one thousand kilometers with limited and continuous chemical variation. Thus, the dykes are more likely to be from a plume.

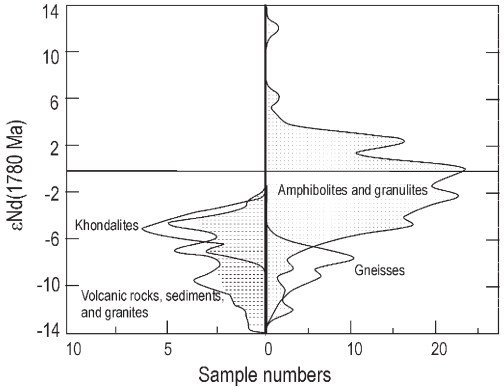

Fig. 13. εNd_t ratios of early Precambrian rocks in the central NCC.

The magma sources of the two generations are presented by the LT Group (EM-I: lower mantle source, contaminated with lithospheric and/or crustal materials) and the HT Group (DM-PREMA: asthenospheric source+varies amounts of lower mantle source, contaminated with lithospheric and/or crustal materials), respectively. We think that the magma source is changed accompanying the evolution of a palaeo-plume: the EM-I type source could be melts mostly from the lower mantle going with the plume head, whereas the DM type source could be melts from the asthenosphere entrained by the plume tail. The 1st generation is widespread, whereas the 2nd generation is scarcely distributed. This indicates that the magma tapped by the plume tail is quite less than that from the head. Although there are some experimental and numerical models of plumes that show that a plume head may carry large amounts of surrounding materials (no matter lithospheric or asthenospheric materials), whereas the plume tail typically entrains little surrounding materials because of a temperature decrease and buoyancy increase (e.g. Kellogg and King, 1993; Hauri et al., 1994). Some new observations reveal that a plume head may contain the source material, whereas the plume tail largely or partly entrains surroundings, depending on the viscosity (e.g. van Keken, 1997; Davis, 1999). A case study from the Arabian–Nubian shield shows another example that the asthenospheric melts are included late (e.g. Stein and Hofmann, 1992). In addition, observations from the Hawaiian Islands also show a DM source comes after an EM-I source (e.g. Wyllie,

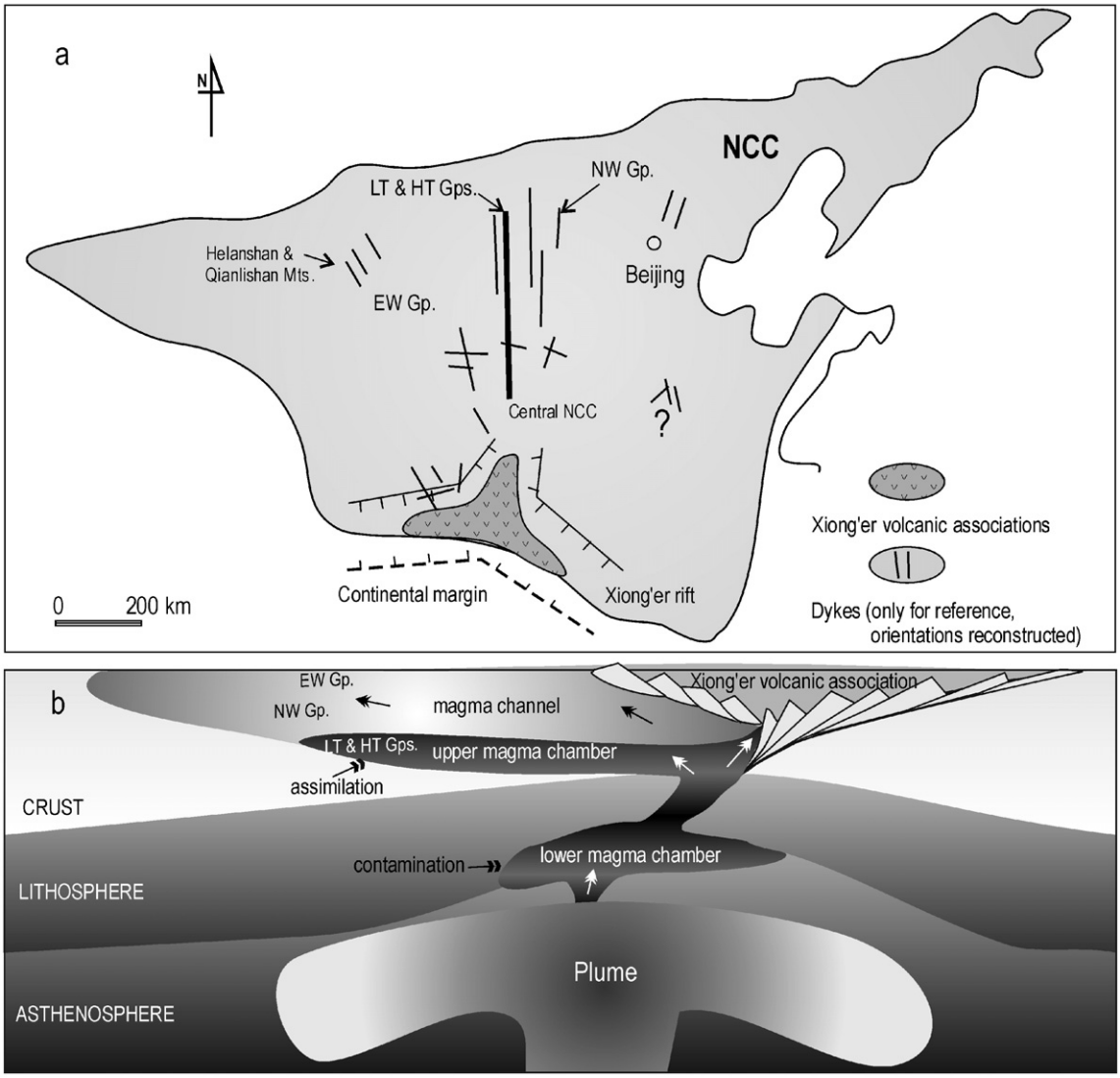

Fig. 14. Petrogenesis cartoons of the dykes in the central NCC; (a) sketch geological map; (b) section view of the magmatic process. The directions of the dykes are reconstructed after Peng et al. (2006).

1988); although there are different opinions about the homes of the DM and EM-I sources.

The plume center was probably located under or around the Xiong'er tripled-rift system in the south margin NCC. These other two arms of the plume-fed rift system opened successfully to form the Qinling Ocean (e.g., Kusky and Li, 2003). The EW-trending dykes (the EW Group) cut cross or turned continuously to the NW-trending dykes (the NW Group). Some dykes have an angle of about 60 degrees (e.g. in Zhongtiaoshan Mts.), but some are subvertical (e.g. in Lvliangshan Mts.). These dykes are parallel or subvertical to one branch of the triple rift. We suggest that these dykes could have intruded along some kinds of fractures in the upper crustal level during uplift (Fig. 14a), as the stress field may change its orientation when the dykes reach the upper most level (Ernst et al., 1995). Or it is controlled by the arm of the Xiong'er rift which is elongated into the central NCC. We also notice that the LT and HT dykes are restricted within a limited belt area, corresponding to one branch of the Xiong'er rift which penetrated into the central NCC (Fig. 14a). This belt could be the upper magma chamber direction and the magma of their associated dykes (the LT and HT Groups) and their descendents (the NW and EW Groups) are extruded from this belt. Fig. 14b shows the possible processes: contamination of lithospheric melts at the lower magma chamber, crustal assimilation and crystallization in the upper magma chamber (e.g. the LT and HT Groups), fractional crystallization process in the magma channels (e.g. the NW Group) and even fluid contamination in the upper part of the channels (e.g. the EW Group).

The Xiong'er triple-armed rift along the southern margin NCC contacts with the Mesozoic Qinling–Dabie orogenic belt. There are massive continental-margin sediments right above the Xiong'er volcanics in the stratigraphy of this rift initiated at the beginning of Mesoproterozoic. After the sedimental deposition, there were few magmatic activities until the collision time of the Qinling–Dabie Orogen (e.g. Zhai et al., 2003b). This fact indicates a long time span of continental margin evolution for the south margin of the NCC from Mesoproterozoic (ca. 1.75 Ga/1.70 Ga) to late Triassic. Moreover, the sediments in-between

the Xiong'er volcanics are river–lake-facies. This observation suggests that the south margin of the NCC became a continental margin right after the Xiong'er volcanism between 1.75 and 1.80 Ga. We believe that the NCC was therefore broken from other block(s) at ca. 1.78 Ga. The North China giant dyke swarms, together with the coeval dykes from other old block(s), could be originally a giant radiating dyke swarm dismembered at ca. 1.78 Ga. Peng et al. (2005) suggested that the dykes in the NCC and the Dharwar craton could constitute a giant dyke swarm. This break-up event could even have contributed to the evolution of the Palaeoproterozoic supercontinent at that time.

Acknowledgements

This research was supported by the National Science Foundation of China (Grant Nos. 40473018, 40234050, 40372089, 40602024 and 40472047), Key Laboratory of Orogenic Belts and Crustal Evolution, Peking University, and U.S. National Science Foundation awards 02-07886 and 01-25925 awarded to T. Kusky. We appreciate discussions with Dr. H. Halls, Dr. J.-H. Li, Dr. G.-C. Zhao and Dr. F.-K. Chen. Thanks for critical reviews by Dr. S.-W. Liu and Dr. G.-C. Zhao and helpful support by Dr. M. Santosh and Dr. W.-J. Xiao.

References

Abbott, D.H., Isley, A.E., 2002. The intensity, occurrence, and duration of superplume events and eras over geological time. Journal of Geodynamics 34, 265–307.

Arndt, N.T., Christensen, U., 1992. The role of lithospheric mantle in continental flood volcanism: thermal and geochemical constraints. Journal of Geophysical Research 97 (B7), 10967–10981.

Brooks, K.C., Larsen, L.M., Nielsen, T.F.D., 1991. Important of iron-rich tholeiitic magmas at divergent plate margins: a reappraisal. Geology 19, 269–272.

Blundy, J.D., Holland, T.J.B., 1990. Calcic amphibole equilibria and a new amphibole-plagioclase geothermometer. Contributions to Mineralogy and Petrology 104, 208–224.

Bohlen, S.R., Batcher, A.L., 1981. Experimental investigations and geological applications of orthopyroxene geobarometry. American Mineralogist 66, 951–964.

Brey, G.T., Kohler, T., 1990. Geothermo-barometry in four phase lherzolites, part II: new thermo- barometers, and practical assessment of existing thermobarometers. Journal of Petrology 31, 1353–1378.

Chen, F.-K., Hegner, E., Todt, W., 2000. Zircon ages, Nd isotopic and chemical compositions of orthogneisses from the Black Forest, Germany—evidence for a Cambrian magmatic arc. International Journal of Earth Sciences 88, 791–802.

Compbell, I.H., 2001. Identification of ancient mantle plume. In: Ernst, R.E., Buchan, K.L. (Eds.), Mantle Plume: Their Identification Through Time, vol. 352. Geological Society of America Special Paper, Boulder, Colorado, 5–21.

Davis, G.F., 1999. Dynamic Earth Plates, Plumes and Mantle Convection. Cambridge University Press, Cambridge, UK. 455 p.

Ernst, R.E., Head, J.W., Parfitt, E., Grosfils, E., Wilson, L., 1995. Giant radiating dyke swarms on Earth and Venus. Earth-Science Review 39, 1–58.

Gallagher, K., Hawkesworth, C., 1992. Dehydration melting and the generation of continental flood basalts. Nature 358, 57–59.

Gibson, S.A., Thompson, R.N., Dickin, A.P., 2000. Ferropicrites: geochemical evidence for Fe-rich streaks in upwelling mantle plumes. Earth and Planetary Science Letters 174, 355–374.

Guo, J.-H., Sun, M., Chen, F.-K., Zhai, M.-G., 2005. Sm–Nd and SHRIMP U–Pb zircon geochronology of high-pressure granulites in the Sanggan area, North China craton: timing of Paleoproterozoic continental collision. Journal of Asian Earth Sciences 24 (5), 629–642.

Halls, H.C., Li, J.-H., Davis, D., Hou, G.-T., Zhang, B.-X., Qian, X.-L., 2000. A precisely dated Proterozoic paleomagnetic pole form the North China craton, and its relevance to paleocontinental construction. Geophysical Journal International 143, 185–203.

Hart, S.R., 1988. Heterogeneous mantle domains: signatures, genesis and mixing chronologies. Earth and Planetary Science Letters 90, 273–296.

Hauri, E.H., Whitehead, J.A., Hart, S.R., 1994. Fluid dynamic and geochemical aspects of entrainment in mantle plumes. Journal of Geophysics Research 99 (24), 275–300.

Hoang, N., Flower, M.F.J., Carlson, R.W., 1996. Major, trace element, and isotopic compositions of Vietnamese basalts: interaction of hydrous EM1-rich asthenosphere with thinned Eurasian lithosphere. Geochimica et Cosmochimica Acta 60, 4329–4351.

Hollister, L.S., Grissom, G.C., Peters, E.K., Stowell, H.H., Sisson, V.B., 1987. Confirmation of the empirical correlation of Al in hornblende with pressure of solidification of calc-alkaline plutons. American Mineralogist 72, 231–239.

Hou, G.-T., Li, J.-H., Qian, X.-L., 2001. Geochemical characteristics and tectonic setting of Mesoproterozoic dyke swarms in northern Shanxi. Acta Petrologica Sinica 17 (3), 352–357 (in Chinese with English Abstract).

Hunter, R.H., Sparks, R.S.J., 1987. The differentiation of the Skaergaard intrusion. Contribution to Mineralogy and Petrology 95, 451–461.

Juster, T.C., Grove, T.L., Perfit, M.R., 1989. Experimental constraints on the generation of Fe–Ti basalts, andesites, and rhyodacites at the Galapagos Spreading Center, 85°W and 95°W. Journal of Geophysical Research 94, 9251–9274.

Kellogg, L.H., King, S.D., 1993. Effect of mantle plumes on the growth of D″ by reaction between the core and mantle. Geophysical Research Letters 20, 379–382.

Kröner, A., Wilde, S.A., Li, J.-H., Wang, K.-Y., 2005. Age and evolution of a late Archaean to Paleoproterozoic upper to lower crustal section in the Wutaishan/Hengshan/Fuping terrain of north China. Journal of Asian Earth Sciences 24 (5), 576–577.

Kusky, T.M., Li, J.-H., 2003. Paleoproterozoic tectonic evolution of the North China craton. Journal of Asian Earth Sciences 22, 383–397.

Kusky, T.M., Li, J.-H, Tucker, R.T., 2001. The Archaean Dongwazi ophiolite complex, North China craton: 2.505 billion year old oceanic crust and mantle. Science 292, 1142–1145.

Kusky, T.M., Windley, B.F., Zhai, M.-G., in press. Mesozoic Sub-Continental Lithospheric Thinning Under Eastern Asia, Preface. In: Zhai, M.-G., Windley, B.F., Kusky, T.M., Meng, Q.-R. (Eds.), Mesozoic Sub-Continental Lithospheric Thinning Under Eastern Asia, Geological Society of London Special Publication.

Kusky, T.M., Windley, B.F., Zhai, M.-G., in press. Tectonic evolution of the North China block: from orogen to craton to orogen. In: Zhai, M.-G., Windley, B.F., Kusky, T.M., Meng, Q.-R. (Eds.), Mesozoic Sub-Continental Lithospheric Thinning Under Eastern Asia, Geological Society of London Special Publication.

Kusky, T.M., Windley, B.F., Zhai, M.-G., in press. Mesozoic sub-continental lithospheric thinning under eastern Asia, lithospheric thinning in eastern Asia: constraints, evolution, and tests of models. In: Zhai, M.-G., Windley, B.F., Kusky, T.M., Meng, Q.-R., (Eds.), Mesozoic Sub-Continental Lithospheric Thinning Under Eastern Asia, Geological Society of London Special Publication.

le Roex, A.P., Dick, H.J.B., 1981. Petrography and geochemistry of basaltic rocks from the Conrad fracture zone on the America–Antarctica Ridge. Earth and Planetary Science Letters 54, 117–138.

le Roex, A.P., Dick, H.J.B., Reid, A.M., Erlank, A.J., 1982. Ferrobasalts from the Spiess Ridge segment of the Southwest Indian Ridge. Earth and Planetary Science Letters 60, 437–451.

Leybourne, M.I., Wagoner, N.V., Ayres, L.D., 1999. Partial melting of a refractory subducted slab in a Paleoproterozoic island arc: implications for global chemical cycles. Geology 27 (8), 731–734.

Li, J.-H., Hou, G.-T., Qian, X.-L., Halls, H.C., Don, D., 2001. Single-zircon U–Pb age of the initial Mesoproterozoic basic dyke swarms in Hengshan Mountain and its implication for the tectonic evolution of the North China craton. Geological Review 47 (3), 234–238 (in Chinese with English Abstract).

Li, J.-H., Kusky, T.M., Huang, X.-N., 2002. Neoarchaean podiform chromitites and mantle tectonites in ophiolitic mélange, North China craton: a record of early Oceanic mantle oceanic mantle processes. GSA Today 12, 4–11.

Lu, S.-N., Yang, C.-L., Li, H.-K., Li, H.-M., 2002. A group of rifting events in the terminal Paleoproterozoic in the North China craton. Gondwana Research 5, 123–131.

Mahoney, J.J., 1988. Deccan traps. In: MacDougall, J.D. (Ed.), Continental Flood Basalt. Kluwer Acad. Publ, 151–194.

Markl, G., Foster, C.T., Bucher, K., 1998. Diffusion-controlled Olivine Corona Textures in Granitic Rocks From Lofoten, Norway: Calculation of Onsager Diffusion Coefficients Thermodynamic Modeling and Petrological Implications.

McBirney, A.T., 1989. The Skaergaard layered series: I. Structure and average compositions. Journal of Petrology 30 (2), 297–363.

Menzies, M.A., 1992. The lower lithosphere as a major source for continental flood basalts: a re-appraisal. In: Storey, B.C., Alabaster, T., Pankhurst, R.J. (Eds.), Magmatism and Causes of Continental Break-up. The Geological Society, London, 31–40.

Pearce, T.H., Gorman, B.E., Birkett, T.C., 1975. The TiO_2–K_2O–P_2O_5 diagram: a method of discriminating between oceanic and non-oceanic basalts. Earth and Planetary Science Letters 24, 419–426.

Peng, P., 2005. Petrogenesis and tectonic significance of the ca. 1.8 Ga mafic dyke swarms in the central North China craton. Doctoral paper, Institute of Geology and Geophysics, Chinese Academy of Sciences, Beijing, 1–213 (in Chinese with English abstract).

Peng, P., Zhai, M.-G., Zhang, H.-F., Zhao, T.-P., Ni, Z.-Y., 2004. Geochemistry and geological significance of the 1.8 Ga mafic dyke swarms in the North China craton: an example from the Juncture of Shanxi, Hebei and Inner-Mongolia. Acta Petrologica Sinica 20 (3), 439–456 (in Chinese with English abstract).

Peng, P., Zhai, M.-G., Zhang, H.-F., Guo, J.-H., 2005. Geochronological constraints on the Paleoproterozoic evolution of the North China craton: SHRIMP zircon ages of different types of mafic dikes. International Geology Review 47 (5), 492–508.

Peng, P., Zhai, M.-G., Guo, J.-H., 2006. 1.80–1.75 Ga mafic dyke swarms in the central North China craton: implications for a plume-related break-up event. In: Hanski, E., Mertanen, S., Ramö, T., Vuollo, J. (Eds.), Dyke Swarms—Time Markers of Crustal Evolution. A.A. Balkema Publishers.

Polat, A., Kusky, T.M., Li, J.H., Fryer, B, Kerrich, R, Patrick, K., 2005. Geochemistry of Neoarchean (ca. 2.55–2.50 Ga) volcanic and ophiolitic rocks in the Wutaishan Greenstone Belt, Central Orogenic Belt, North China Craton: implications for geodynamic setting and continental growth. Geological Society of America Bulletin 117, 1387–1399.

Polat, A., Herzberg, C., Munker, C., Rodgers, R., Kusky, T., Li, J.H., Fryer, B., Delany, J., 2006. Geochemical and petrological evidence for a suprasubduction zone origin of Neoarchean (ca. 2.5 Ga) peridotites, central orogenic belt, North China craton. Bulletin of the Geological Society of America 118, 771–784.

Qian, X.-L., Chen, Y.-P., 1987. Late Precambrian mafic dyke swarms of the North China craton. In: Halls, H.C., Fahrig, W.F. (Eds.), Mafic Dyke Swarms. Geology Association of Canada Special Paper, 34, 385–391.

Rogers, J.J.W., Santosh, M., 2002. Configuration of Columbia, a Mesoproterozoic supercontinent. Gondwana Research 5, 123–132.

Rollinson, H., 1995. Using geochemical data, evaluation, presentation, and interpretation. Longman Scientific and Technical 63, 108.

Russell, J.K., Nicholls, J., 1988. Analysis of petrological hypotheses with Pearce element ratios. Contribution to Mineralogy and Petrology 99, 25–35.

Snyder, D., Carmichael, I.S.E., Wiebe, R.A., 1993. Experimental study of evolution in a Fe-rich, layered mafic intrusion: constraints of Fe–Ti oxide precipitation on the T-f_{O2} and T-ρ paths of tholeiitic magmas. Contribution to Mineralogy and Petrology 113, 73–86.

Stein, M., Hofmann, A.W., 1992. Fossil plume head beneath the Arabian lithosphere? Earth and Planetary Science Letters 144, 193–209.

Sun, S.-S., McDonough, W.F., 1989. Chemical and isotopic systematics of oceanic basalts implications for mantle composition and process. In: Saunders, A.D., Nony, M.J. (Eds.), Magmatism in the Ocean Basins. Geological Society Special Publication, 42, 313–354.

Toplis, M.J., Carroll, M.R., 1995. An experimental study of the influence of oxygen fugacity on Fe–Ti oxide stability, phase relations, and mineral-melt equilibria in ferro-basaltic systems. Journal of Petrology 36, 1137–1170.

Toplis, M.J., Carroll, M.R., 1996. Differentiation of ferro-basaltic magmas under conditions open and closed to oxygen: implications for the Skaergaard intrusion and other natural systems. Journal of Petrology 37, 837–858.

van Keken, P., 1997. Evolution of starting mantle plumes: a comparison between numerical and laboratory models. Earth and Planetary Science Letters 148, 1–11.

Wan, Y.-S., Zhang, Q.-D., Song, T.-R., 2003. SHRIMP ages of detrital zircons from the Changcheng System in the Ming Tombs area, Beijing: constraints on the protolith nature and maximum depositional age of the Mesoproterozoic cover of the North China craton. Chinese Science Bulletin 48 (22), 2500–2506.

Wang, S.-S., Sang, H.-Q., Qiu, J., Cheng, M.-E., Li, M.-R., 1995. The metamorphic age of pre-Changcheng system in Beijing–Tianjin area and a discussion about the lower limit age of Changcheng system. Scientia Geologica Sinica 3 (4), 348–354.

Wang, Y.-J., Fan, W.-M., Zhang, Y.-H., Guo, F, Zhang, H.-F., Peng, T.-P., 2004. Geochemical, $^{40}Ar/^{39}Ar$ geochronological and Sr–Nd isotopic constraints on the origin of Paleoproterozoic mafic dikes from the southern Taihang Mountains and implications for the ca. 1800 Ma event of the North China craton. Precambrian Research 135, 55–77.

Wiebe, R.A., 1997. Fe-rich tholeiitic liquids and their cumulate products in the Pleasant Bay layered intrusion, coastal Maine. Contributions to Mineralogy and Petrology 167, 255–267.

Wilde, S.A., Zhao, G.-C., Sun, M., 2002. Development of the North China craton during the Late Archaean and its final amalgamation at 1.8 Ga: some speculation on its position within a global Paleoproterozoic Supercontinent. Gondwana Research 5, 85–94.

Wyllie, 1988. Magma genesis, plate tectonics and chemical differentiation of the Earth. Reviews of Geophysics 26, 370–404.

Wu, C.-H., Zhang, C.-T., 1998. The Paleoproterozoic SW–NE collision model for the central North China craton. Progress of Precambrian Research 21, 28–50 (in Chinese with English abstract).

Wu, F.-Y., Zhao, G.-C., Wilde, S.A., Sun, D.-Y., 2005. Nd isotopic constraints on crustal formation in the North China craton. Journal of Asia Earth Sciences 24 (5), 523–546.

Xu, Y.-G., Mei, H.-J., Xu, J.-F., Huang, X.-L., Wang, Y.-J., Chung, S.-L., 2003. Origin of two differentiation trends in the Emeishan flood basalts. Chinese Science Bulletin 48, 390–394.

Zhai, M.-G., Guo, J.-H., Li, Y.-G., Liu, W.-J., Peng, P., Shi, X., 2003a. Two linear granite belts in the central-western North China craton and their implication for late Neoarchaean–Paleoproterozoic continental evolution. Precambrian Research 127, 267–283.

Zhai, M.-G., Zhu, R.-X., Liu, J.-M., Meng, Q.-R., Hou, Q.-L., Hu, S.-B., Li, Z., Zhang, H.-F., Liu, W., 2003b. Time range of Mesozoic tectonic regime inversion in eastern North China Block. Science in China. Series D 47 (2), 151–159.

Zhao, G.-C., Sun, M., Wilde, S.A., 2002a. Review of global 2.1–1.8 Ga orogens: implications for a pre-Rodinia supercontinent. Earth-Science Reviews 59, 125–162.

Zhao, G.-C., Wilde, S.A., Cawood, P.A., Sun, M., 2001. Archaean blocks and their boundaries in the North China craton: lithological, geochemical, structural and P–T path constraints and tectonic evolution. Precambrian Research 107, 45–73.

Zhao, G.-C., Wilde, S.A., Cawood, P.A., Lu, L.-Z., 1998. Thermal evolution of the Archaean basement rocks from the eastern part of the North China craton and its bearing on tectonic setting. International Geological Review 40, 706–721.

Zhao, T.-P., Zhai, M.-G., Xia, B., Li, H.-M., Zhang, Y.-X., Wang, Y.-S., 2004. Zircon U–Pb SHRIMP dating for the volcanic rocks of the Xiong'er Group: Constraints on the initial formation age of the cover of the North China craton. Chinese Science Bulletin 49 (23), 2495–2502.

Zhao, T.-P., Zhou, M.-F., Zhai, M.-G., Xia, B., 2002b. Paleoproterozoic rift-related volcanism of the Xiong'er group, North China craton: implications for the breakup of Columbia. International Geology Review 44, 336–351.